**Atmospheric
Chemistry
and Physics
Discussions**

Drivers of hemispheric differences in return dates of mid-latitude stratospheric ozone to historical levels

H. Garny[1], G. E. Bodeker[2], D. Smale[3], M. Dameris[1], and V. Grewe[1]

[1]Deutsches Zentrum für Luft- und Raumfahrt, Institut für Physik der Atmosphäre, Oberpfaffenhofen, Germany
[2]Bodeker Scientific, Alexandra, New Zealand
[3]NIWA Lauder, New Zealand

Correspondence to: H. Garny (hella.garny@dlr.de)

Title Page

Abstract	Introduction
Conclusions	References
Tables	Figures

| I◄ | ►I |
| ◄ | ► |

Back | Close

Full Screen / Esc

Printer-friendly Version

Interactive Discussion

Abstract

Chemistry-climate models (CCMs) project an earlier return of northern mid-latitude to-
tal column ozone to 1980 values compared to the southern mid-latitudes. The chemical
and dynamical drivers of this hemispheric difference are investigated in this study. The
hemispheric asymmetry in return dates is a robust result across different CCMs and
is qualitatively independent of the method used to estimate return dates. However,
the differences in dates of return to 1980 levels between the southern and northern
mid-latitudes can vary between 0 and 30 yr across the range of CCM projections ana-
lyzed. An attribution analysis performed with two CCMs shows that chemically-induced
changes in ozone are the major driver of the earlier return of ozone to 1980 levels in
northern mid-latitudes; transport changes are of minor importance. This conclusion is
supported by the fact that the spread in the simulated hemispheric difference in return
dates across an ensemble of twelve models is only weakly related to the spread in
the simulated hemispheric asymmetry of trends in the strength of the Brewer–Dobson
circulation. The causes for chemically-induced asymmetric ozone trends relevant for
the total column ozone return date differences are found to be (i) stronger increases in
ozone production due to enhanced NO_x concentrations in the Northern Hemisphere
lowermost stratosphere and troposphere, (ii) stronger decreases in the destruction
rates of ozone by the NO_x cycle in the Northern Hemisphere lower stratosphere linked
to effects of dynamics and temperature on NO_x concentrations and (iii) an increas-
ing efficiency of heterogeneous ozone destruction by Cl_y in the Southern Hemisphere
mid-latitudes as a result of decreasing temperatures.

1 Introduction

In support of the WMO/UNEP ozone assessment 2010 (WMO, 2011), the SPARC
(Stratospheric Processes And their Role in Climate) CCMVal-2 activity coordinated
simulations of the future evolution of atmospheric ozone using about a dozen

Title Page

Abstract | Introduction

Conclusions | References

Tables | Figures

◄◄ | ►►

◄ | ►

Back | Close

Full Screen / Esc

Printer-friendly Version

Interactive Discussion

chemistry-climate models (CCMs). These simulations have been extensively analyzed and evaluated (SPARC-CCMVal, 2010). As a result of the success of the Montreal Protocol and its amendments and adjustments, tropospheric concentrations of ozone depleting substances (ODSs) are decreasing (Montzka et al., 1999) and are expected to continue to decrease over the next century. In mid-latitudes, stratospheric Cl_y is projected by CCMs to return to 1980 levels by the middle of the 21st century. Total column ozone (TOZ), on the other hand, is projected by CCMs to return to 1980 values earlier; by the early 2020s over northern mid-latitudes and by the mid-2030s over southern mid-latitudes (Austin et al., 2010; Eyring et al., 2010). Unlike Cl_y where the return to 1980 values is hemispherically symmetric (Austin et al., 2010), the return of TOZ to 1980 values is hemispherically asymmetric. In Austin et al. (2010) and Oman et al. (2010) it was shown that this hemispheric asymmetry results from changes in lower stratospheric ozone, specifically ozone below 20 hPa.

In addition to being influenced by ozone depleting substances (ODSs), ozone concentrations are also affected by changes in greenhouse gas (GHG) concentrations. While ODS concentrations increased strongly in the second half of the 20th century, and are expected to decline again in the 21st century, GHG concentrations are projected to keep rising monotonically. Eyring et al. (2010) used a multi-model set of sensitivity simulations, in which either ODS or GHG concentrations were held constant, to show that the hemispheric difference in mid-latitude ozone evolution is due to a stronger response of Northern Hemisphere (NH) ozone to increasing GHG concentrations compared to its Southern Hemisphere (SH) counterpart.

A number of processes determine the response of mid-latitude ozone to increasing GHG concentrations. In the upper stratosphere, increasing GHG concentrations cause temperatures to decrease which slows the $O + O_3 \rightarrow 2O_2$ reaction such that ozone increases (Portmann and Solomon, 2007). Increases in the concentrations of N_2O and CH_4 elevate the concentrations of the ozone precursors NO_x ($= NO + NO_2$) and HO_x ($= H + OH + HO_2$). However, the response of ozone to changes in N_2O and CH_4 depends on a number of coupled processes. For example, the ratio of NO_x to

N$_2$O is temperature-dependent, such that decreasing temperatures lower the yield of NO$_x$ from N$_2$O (Plummer et al., 2010; Revell et al., 2012b). The speed and path of air parcels through the Brewer–Dobson Circulation (BDC) also affects NO$_x$ concentrations by determining the time available for photolysis of N$_2$O (Cook and Roscoe, 2012). Since CCMs consistently project a strengthening of the BDC (Butchart et al., 2010), this will also reduce the yield of NO$_x$ from N$_2$O (Cook and Roscoe, 2012).

In previous studies, the hemispheric asymmetry in the response of ozone to increasing GHG concentrations was attributed to hemispheric asymmetries in changes in transport; the strength of the BDC is projected to increase more in the NH compared to the SH (WMO, 2011; Eyring et al., 2010; Austin et al., 2010). However, little evidence has been presented to support this hypothesis. In this study, the role of changes in transport on the hemispheric asymmetry of return dates of mid-latitude ozone to 1980 levels is reassessed. Two complementary approaches are followed: first, a multi-model ensemble of CCMVal-2 models is used to investigate the robustness of projections of the temporal evolution of ozone, and then two CCMs (described in Sect. 2), that incorporate the necessary diagnostics, are used to conduct a detailed attribution of the drivers of mid-latitude ozone changes through the 21st century. These diagnostics, along with other methods used in the analysis, are described in Sect. 3. In Sect. 4, the multi-model analysis is presented, testing the consistency of the hemispheric asymmetry in return dates across models, and evaluating the height dependence of the hemispheric differences. Based on two of the CCMs, an attribution is performed, allowing an explicit separation of the effects of chemistry and transport (Sect. 5). The chemically-induced ozone changes and their drivers are analyzed in more detail in Sect. 6. Uncertainties and the relevance of the processes found are discussed in Sect. 7. Conclusions are presented in Sect. 8.

2   Chemistry-climate models

Within CCMVal-2 (SPARC-CCMVal, 2010) a set of simulations was performed with a number of CCMs aiming at investigating the stratospheric ozone layer. Our analysis requires seamless simulations from the past to the future, and the necessary output of these simulations was available from 12 CCMs. The individual models are not identified as this is not required for the analyses that aim to explore the spread in the simulations rather than the performance of individual models. A description of models and the simulation set-ups can be found in Morgenstern et al. (2010). For 10 of the models, REF-B2 simulations are analyzed while SCN-B2d simulations are analyzed for the remaining two. The SCN-B2d simulation differs from REF-B2 in that it includes natural variability, i.e. the solar cycle and the QBO (see Eyring et al., 2008). However, for the purposes of this study, the two simulations are equivalent.

Two CCMs, that are equipped with the necessary diagnostics, are used more extensively for the attribution analysis and are described in greater detail below.

2.1   NIWA-SOCOL

The NIWA-SOCOL (National Institute of Water and Atmospheric Research – SOlar Climate Ozone Links) CCM is a modified version of the CCM SOCOL_v2.0 (Schraner et al., 2008) in which stratospheric ozone is simulated including a budget analysis of ozone production, loss from different catalytic cycles and transport. SOCOL comprises the MAECHAM4 global climate model and a modified version of the chemistry transport model MEZON (Egorova et al., 2003). MAECHAM4 is configured with a T30 spectral horizontal resolution with 39 vertical levels between Earth's surface and 0.01 hPa ($\sim$ 80 km). A hybrid transport scheme is employed to advect the chemical constituents. The chemical solver algorithm uses a Newton–Raphson iterative method, taking into account 41 chemical species, 140 gas-phase reactions, 46 photolysis reactions and 16 heterogeneous reactions.

Ozone return dates

H. Garny et al.

The output used in this study originates from a NIWA-SOCOL REF-B2 simulation. This simulation is an updated version of the one performed for the SPARC CCMVal-2 activity in that the sea surfaces temperatures (SSTs) simulated by ECHAM5-MPI-OM are used. Otherwise the boundary conditions are as described in Morgenstern et al. (2010) and are consistent with the CCMVal-2 specifications. In the NIWA-SOCOL simulation, a minor error was made in the prescription of the NO_x boundary condition i.e. aircraft NO_x emissions were inadvertently doubled. However, since NIWA-SOCOL is used to study ozone changes mostly above 100 hPa this error is not expected to impact the results.

A diagnostic implemented within the model tracks the change in the ozone concentration within each model grid cell, at each time step, resulting from net chemical production and net transport into the cell. The change in net chemical production is calculated explicitly, and can be further attributed to different catalytic cycles. Further attribution of odd oxygen $(O + O_3)$ production, via the Chapman cycles, and destruction by the HO_x, NO_x and Cl_y cycles, across 15 different catalytic cycles, was performed within the model chemistry scheme using the rate limiting steps of the corresponding reaction cycles. This diagnostic, along with the detailed list of reaction cycles, is described in Revell et al. (2012b). In this paper, destruction by bromine-containing species is included in the Cl_y destruction term. The change in ozone due to transport is defined as the residual of the net chemical production subtracted from the total ozone change. Both terms are recorded and accumulated into monthly means for each grid cell. Since transport is determined as a residual, any numerical computation residual and renormalization of the ozone concentrations are folded into the transport term.

2.2 E39CA

The CCM ECHAM4.L39(DLR)/CHEM/ATTILA (E39CA) is an updated version of ECHAM4.L39(DLR)/CHEM (E39C) (Hein et al., 2001; Dameris et al., 2005) with the former semi-Lagrangian advection scheme replaced by the fully Lagrangian advection scheme ATTILA (Reithmeier and Sausen, 2002; Stenke et al., 2009). E39C is based on

the spectral general circulation model ECHAM4.L39(DLR) (Land et al., 2002) and the chemistry-module CHEM (Steil et al., 1998). The model is run with a spectral horizontal resolution of T30, corresponding to ~ 3.75° × 3.75° on a transformed latitude-longitude grid. The model consists of 39 layers in the vertical, extending from the surface to the uppermost layer centered at 10 hPa. The chemistry module CHEM is based on a generalized family concept and includes homogeneous and stratospheric heterogeneous ozone chemistry and the most relevant chemical processes for describing tropospheric background chemistry. Ozone depletion cycles involving bromine were originally not implemented in the CHEM module, but subsequently a parameterization for the bromine chemistry was included. The parameterization is based on the photolysis of Cl_2O_2 and described in detail in Stenke et al. (2009). Boundary conditions for the two families Cl_x (= $HCl + ClONO_2 + ClO_x$) and NO_y (= $NO_x + HNO_3$) are prescribed at the uppermost model level (10 hPa) to account for chemical processes above the model top. For a more detailed description of E39CA, see Stenke et al. (2009). The SCN-B2d simulation performed with E39CA, as submitted to the CCMVal-2 archives, is used here. The simulation extends from 1960 to 2049, and the boundary conditions including anthropogenic and natural forcings are described in Garny et al. (2009).

As in NIWA-SOCOL, ozone production and destruction rates from a prescribed set of chemical reaction cycles are calculated from the rate limiting reaction steps, and are saved as part of the model output. The total chemical tendencies of ozone are then calculated off-line from the sum of the tendencies of the chemical cycles. The transport tendencies are calculated by subtracting the ozone chemical tendencies from the total ozone tendencies. Thus, transport tendencies are calculated as residuals in both models, in NIWA-SOCOL online during the simulation and in E39CA off-line after the simulation was performed. Therefore, transport tendencies include in both models any spurious contributions to ozone tendencies resulting from numerical artifacts within the model.

Chemical reaction cycles are grouped, as in NIWA-SOCOL, into production by the Chapman cycle, and destruction by the HO_x, NO_x and Cl_y cycles. As mentioned above,

any bromine-related ozone destruction is included in the Cl$_y$ loss term. Additionally, in E39CA the rate limiting reaction rates of two of the main tropospheric ozone production cycles are saved as output. These rate limiting reactions are (1) HO$_2$ + NO → OH + NO$_2$ (in the following referenced as "PHN") and (2) CH$_3$O$_2$ + NO → CH$_3$O + NO$_2$ (referenced as "PCN"). Dry deposition at the surface is also considered for the budget calculation.

3 Methods

3.1 Ozone attribution method

Ozone changes are attributed to sources and sinks (chemical production and loss and transport of ozone) as described in Garny et al. (2011). A short summary of the method is given in the following. The required model output are the chemical ozone tendencies (the total ozone production and the total ozone destruction). In Garny et al. (2011), changes in ozone between two time periods were attributed to changes in chemical production, destruction and transport. It was assumed that the annual mean ozone tendencies, averaged over the period of interest, were close to zero. Here, this method is extended so that it can be applied to time series of ozone, i.e. the method attributes year-to-year changes to changes in the sink and source terms.

The ozone budget equation for the annual mean change in ozone for two periods $p1$ and $p2$ is (see Eq. 4 of Garny et al., 2011):

$$\left[\frac{\partial O_3}{\partial t}\right]^{p_1} = [P]^{p_1} - [DO_3]^{p_1} + [T]^{p_1}$$

$$\left[\frac{\partial O_3}{\partial t}\right]^{p_2} = [P]^{p_2} - [DO_3]^{p_2} + [T]^{p_2}$$

(1)

The integration denoted by [·] is the integral over the time periods p_1 and p_2, respectively. O$_3$ is the ozone mixing ratio within some model grid cell, P is the ozone production within the grid cell, and D is the fraction of the ozone destroyed in that time step

Full Screen / Esc

Printer-friendly Version

Interactive Discussion

within the grid cell. T is the net amount of ozone transported into or out of the grid cell. In contrast to Garny et al. (2011), the term $\left[\frac{\partial O_3}{\partial t}\right]$ is not assumed to be zero, allowing periods to be a single year.

For $[DO_3] \approx [D][O_3]$, the equations above can be transformed to describe the relative change in ozone as:

$$\underbrace{\frac{[O_3]^{p_2} - [O_3]^{p_1}}{[O_3]^{p_1}}}_{\text{rel. ozone change}} = \underbrace{\frac{[D]^{p_1} - [D]^{p_2}}{[D]^{p_2}}}_{\text{Destruction-induced O}_3\text{ change}} + \underbrace{\frac{[P]^{p_2} - [P]^{p_1}}{[P]^{p_1} + [T]^{p_1} - [\Delta]^{p_1}}}_{\text{Production-induced O}_3\text{ change}}$$

$$+ \underbrace{\frac{[T]^{p_2} - [T]^{p_1}}{[P]^{p_1} + [T]^{p_1} - [\Delta]^{p_1}}}_{\text{Transport-induced O}_3\text{ change}} + \underbrace{\frac{[\Delta]^{p_1} - [\Delta]^{p_2}}{[P]^{p_1} + [T]^{p_1} - [\Delta]^{p_1}}}_{\text{Imbalance term}} + \underbrace{\delta D \times \delta P}_{\text{Non-linear, Chemistry}} + \underbrace{\delta D \times (\delta T + \delta\Delta)}_{\text{Non-linear, Mixed}} \tag{2}$$

The first three terms on the right hand side of the equation are the contributions to ozone changes due to changes in destruction, production and transport, respectively. Δ is the the ozone tendency $\left[\frac{\partial O_3}{\partial t}\right]$ averaged over the respective periods, and the fourth term is therefore the contribution to ozone changes due to a difference in the total gain or loss of ozone over one period compared to the other. Hereafter this is referred to as "imbalance" term. The last two terms in the equation describe the nonlinear contributions, where the δ denotes the change in ozone due to changes in the respective source or sink, i.e. the first to fourth terms. The nonlinear terms consist of the changes in the destruction rates applied to all other terms (production, transport and the imbalance term). For example, if there is more ozone production from some chemical cycle during a time step, but it is accompanied by an enhanced destruction rate from a different cycle during the same time step, the elevated ozone is immediately subjected to the enhanced destruction, reducing the effect of the additional production. Similarly, stronger transport of ozone into a grid cell might also be mitigated by local changes in

Ozone return dates

H. Garny et al.

the ozone destruction rate, as described by the nonlinear term. The nonlinear terms are one order of magnitude smaller than the other change terms, so as long as changes are small (< 0.1), this term is one order of magnitude smaller, and thus not important.

In the analysis presented below, transport and chemically-induced ozone changes are separated. The changes due to transport are diagnosed from the third term in Eq. (2). The changes due to chemistry are the sum of the production, destruction and the first nonlinear term (i.e. the first, second and fifth terms in Eq. 2). Hereafter, when referring to the nonlinear term, only the mixed transport-chemistry term (6th term in Eq. 2) is meant.

In Fig. 1, an example of the application of the method is demonstrated for lower stratospheric, partial column, zonal mean ozone at 45° S from 1960 to 2049. The change in ozone in each year, relative to the mean over the 1960 to 1969 decade, is reasonably well reproduced by the sum of the terms on the right hand side of Eq. (2). The individual components of these terms are shown, indicating the extent to which changes in the respective quantity contribute to the relative change in ozone in a particular year. For example, the red line indicates how much ozone would have changed as a result of changes in transport alone. The largest contributions to ozone changes are from changes in chemistry and transport. The imbalance-term (Δ) has a minor contribution to inter-annual variability and none to the long-term decrease in ozone over this period at this location. The nonlinear term has a negligible contribution in this case.

3.2 Estimation of return dates

To estimate dates of return of ozone to 1980 levels, the time series need to be smoothed to remove the effects of unforced (internal) variability which would otherwise make the return date evaluation susceptible to climate noise. For the analysis in support of the 2010 Ozone Assessment (WMO, 2011), a time-series adaptive model analysis (TSAM) method (Scinocca et al., 2010) was used. This method separates the time series into a smooth signal, and superimposed noise, based on a statistical non-parametric fit. An alternative approach is to iteratively smooth the time series

by applying a $1:2:1$ filter many times. A comparison of the TSAM method with the iterative $1:2:1$ smoothing can be found in the supplement to Chapter 9 of the SPARC CCMVal-2 report (SPARC-CCMVal, 2010). This comparison shows that the multi-model mean estimate of mid-latitude ozone return dates is independent of the method used. For individual models, on the other hand, the choice of the method can lead to large differences in the return dates.

A conceptually different approach to separating the signal from the noise is to apply a linear least squares regression model with given geophysical predictors, i.e. using a-priori information on the known drivers of the long-term changes in ozone. In practice, these predictors are the burden of Cl_y (known to be the cause of large depletion of ozone) and a linear trend, which is assumed to approximately represent the response to changes in GHG concentrations and other emissions that increase monotonically (e.g. NO_x emissions at the surface). While this regression approach might be criticized for assuming ozone to be driven only by Cl_y or some linear process, it has the advantage of permitting an attribution between these two terms. In particular, if the goal is to understand the deviation of ozone return dates from Cl_y return dates, the regression performed in this way separates the secular evolution of ozone into a component that is congruent with the Cl_y evolution (i.e. returns to 1980 values when Cl_y does) and a component that drives deviations away from the Cl_y return dates. This physical interpretation of the regression model attribution between its two basis functions requires a sufficiently long time series so that the Cl_y and linear trend basis functions are approximately orthogonal. This is achieved by considering the 1960 to 2049 period. The fitted timeseries from this regression model that attributes ozone changes to Cl_y and the linear trend term is then used to estimate return dates to 1980 values. Additionally, the sensitivity of the returns dates to other methods is tested. Three different methods are intercompared, viz.:

1. Simple regression model
   A linear least squares regression of the form

   $$O_3(t) = a_0 + a_1 \times Cl_y(t) + a_2 \times t + R(t)$$

is applied to the annual mean ozone time series from t = 1960 to 2049. Cl_y mixing ratios at 50 hPa and at the same latitude as the ozone time series, are used as the basis function. a_0, a_1 and a_2 are the offset, the Cl_y and the trend regression coefficients, and R is the residual. The uncertainties on the regression coefficients are calculated taking auto-correlation into account.

2. Regression model with quadratic terms
   Again a linear regression model is used, but including Cl_y and trend terms that are quadratic in Cl_y and t:

$$O_3(t) = a_0 + a_1 \times Cl_y(t) + a_2 \times Cl_y(t)^2 + a_3 \times t + a_4 \times t^2 + R(t)$$

These additional terms allow for more degrees of freedom in the fitted time series, but a physical interpretation of the attributed variance is no longer straight-forward.

3. Smoothing with a 1 : 2 : 1 filter
   A 1 : 2 : 1 filter is applied iteratively to the ozone time series 20 times. The number of iterations of applying the filter is chosen as to obtain a smooth time series from which variability in the inter-annual to decadal time scale is removed but the long-term signal is maintained.

Dates of return of TOZ to 1980 values in the mid-latitudes (45–60°) of both hemispheres for twelve different CCMs are shown in Fig. 2. For method 1 and 2, uncertainties on the return dates are calculated based on the uncertainty on the regression fit. The regression model uncertainties are estimated using a bootstrap procedure: first, the regression model is run on the original time series, obtaining the smooth regression fit and the residuals (original data minus fit). Then, a set of 10 000 perturbed time series are constructed by adding noise to the regression fit. The added noise is generated by randomly selecting, with replacement, from the residuals. The regression model is fitted to each of the 10 000 time series, and for each the return date is estimated. The error bars shown are then one standard deviation over these 10 000 return date estimates.

Ozone return dates

H. Garny et al.

Differences in estimated multi-model mean return dates between the three methods are significantly smaller than the return date differences between models. The simple regression (method 1) yields a multi-model mean return date in the NH ∼ 3 yr earlier than the other two methods, but otherwise the agreement is good. For each individual model, however, the differences in return dates can be 5 to 10 yr depending on the method used. Compared to earlier estimates (Austin et al., 2010; Eyring et al., 2010), the multi-model mean return dates derived here are slightly earlier in both hemispheres. This might result from a different choice of the geographical region (60° to 45° N as opposed to 35° N), for reasons explained later, or from a different subset of CCMs used here. However, the 10 to 15 yr earlier return of northern mid-latitude TOZ to 1980 values compared to southern mid-latitude TOZ is in close agreement with estimates by Austin et al. (2010) and Eyring et al. (2010).

The comparison of the TSAM method with the 1 : 2 : 1 iterative smoothing method in SPARC-CCMVal (2010) (see their Fig. 9, S. 49) shows agreement in return dates for the multi-model mean, suggesting that using an iterative 1 : 2 : 1 filter rather than the TSAM method for deriving return dates will not bias the results. However, when comparing return dates (derived using either method) across individual models, significant inter-model differences are found. This suggests that the differences in the estimates from various methods is caused by the large amount of variability in the individual model time series, adding ambiguity to the retrieval of the signal.

The uncertainties in the return date estimates propagate into the hemispheric differences in return dates (see right panel in Fig. 2). All models, but one, simulate earlier return dates in the northern mid-latitudes compared to the southern mid-latitudes. This is true for all three methods when taking the uncertainty into account. Therefore, the earlier return dates in the NH are robust, not depending on the method used for their calculation.

In the multi-model analysis in Sect. 4 the range of return dates estimated using the different methods is used to test the independence of the results with respect to the method used.

Title Page

Abstract | Introduction

Conclusions | References

Tables | Figures

◄ | ►|

◄ | ►

Back | Close

Full Screen / Esc

Printer-friendly Version

Interactive Discussion

For the attribution analysis in Sect. 5, the simple regression model (method 1) is used together with the chemistry-transport attribution described in Sect. 3.1. In this way the analysis combines two different approaches to the attribution: first, the changes in ozone are attributed to changes in the chemistry and transport tendencies. This attribution differentiates between the processes that are responsible for the ozone changes. The method relies only on the sink and source terms for ozone as provided in the model output, and is not based on statistical methods. In a second step, the simple regression model is applied to (i) the time series of ozone changes, (ii) the time series of chemically-induced ozone changes, and (iii) the time series of transport-induced ozone changes. The regression model implements a purely statistical separation between that part of each time series that is congruent with the evolution of Cl_y and that part that is congruent with a linear trend. The regression does not attribute to the different sources and sinks, i.e. both the Cl_y-congruent part and the linear term are driven by changes in both chemistry and transport. For example, while the changes in ozone in the lower stratosphere that are congruent with Cl_y changes will primarily be chemically driven, ozone is also affected by changes in transport, due both to changes in ozone gradients and to modulation of the strength of the circulation.

4 Multi-model analysis

4.1 Height dependence of hemispheric difference in return dates

The dates of return of mid-latitude TOZ to 1980 levels are found to be hemispherically asymmetric in the multi-model mean shown in WMO (2011). Here, we use twelve of the CCMs that were used in the WMO/UNEP ozone assessment to investigate inter-model differences in the asymmetry of the return dates and which altitude regions are primarily responsible for the asymmetry.

Mid-latitude ozone is defined as the area weighted average over the latitude band 45° to 60° of either hemisphere. This is narrower compared to the WMO (2011) definition

of mid-latitude ozone (35° to 60°). As shown in Sect. 5.2, strengthening of the BDC tends to induce negative ozone trends over low latitudes and positive ozone trends at middle to high latitudes. Because the zero trend in ozone is usually around 45° N/S, this is used as the equatorward boundary of the mid-latitudes to minimize any reduction in
5   the diagnosed effects of transport on ozone trends.

The hemispheric differences in return dates of mid-latitude TOZ for the twelve models are shown in the leftmost panel of Fig. 3. The multi-model mean ozone returns to 1980 levels about 13 yr earlier in the NH compared to the SH, in agreement with WMO (2011). However, there is a large spread in the hemispheric differences among the
10 individual models, ranging from 0 to close to 30 yr, depending on the method used to calculate the return date (see Sect. 3.2).

To evaluate the relative contributions of different altitude regions to the hemispheric differences in return dates, partial ozone columns were calculated for (i) the surface to 10 hPa, (ii) the tropopause to 10 hPa and (ii) the region from 100 to 10 hPa. Thus, the
15 altitude domain of regarded ozone columns is stepwise reduced, excluding first the upper stratosphere, further the troposphere and in a third step also the lowermost stratosphere (i.e. region between the tropopause and 100 hPa). As shown in Fig. 3, excluding the region above 10 hPa slightly amplifies the hemispheric asymmetry in return dates. As ozone above 10 hPa is primarily chemically controlled and ozone changes tend to
20 be correlated with temperature changes which are generally hemispherically symmetric, including the region above 10 hPa obscures some of the hemispheric asymmetry. Additionally excluding the tropospheric ozone column also has a small effect, in this case slightly reducing the hemispheric asymmetry in return dates. As shown by the rightmost column in Fig. 3, the hemispheric asymmetry induced by tropospheric ozone
25 shows a large spread between models that even show differences in sign. Given that tropospheric chemistry is treated quite differently, and in many cases rather simplistically in the CCMs, the large spread is not surprising. The contribution of the lowermost stratosphere (LMSTR; hereafter defined as the layer between the tropopause and 100 hPa), on the other hand, accounts for about half of the hemispheric difference in

return dates (the exact contribution depending on the method used to determine the return date). In all but two models, excluding the LMSTR causes the hemispheric differences in return dates to decrease. Ozone evolution in the lower stratosphere (LSTR; 100 to 10 hPa) accounts for the other half of the hemispheric difference in the return dates. A large spread between the models is found in the LSTR, and in about half the models the hemispheric difference is only marginally significant when considering the uncertainty resulting from the different methods used to calculate 1980 return dates. These results suggests that it is the LMSTR and LSTR that make the largest contribution to the hemispheric asymmetry in TOZ return dates, in agreement with Oman et al. (2010) and Austin et al. (2010). However, large model-to-model differences and uncertainties in return date estimates exist.

To study the altitude dependence of the asymmetry in more detail, the regression model (method 1) was fitted to the partial ozone column time series from each model. As shown by Eyring et al. (2010), in simulations where only ODS concentrations are allowed to vary, while GHG concentrations are held constant, the response of ozone to ODSs (or Cl_y) is approximately linear. The Cl_y fit coefficient can therefore be interpreted as the response of ozone to changes in Cl_y alone, as would result from a "fixed GHG" simulation. As shown in Fig. 2, the multi-model mean Cl_y returns to 1980 levels at the same time in each hemisphere. The hemispheric asymmetry in ozone return dates can in none of the models be fully explained by Cl_y return date differences. Therefore, the variance in TOZ attributed by the regression model to the Cl_y basis function cannot contribute to the hemispheric asymmetry in return dates of ozone. The asymmetry must, therefore, be due to hemispheric differences in the linear trends in ozone as determined by the regression model. Understanding the origin of linear trends in ozone in both hemispheres over the period 1960 to 2049 is therefore likely to lead to an explanation of the hemispheric differences in TOZ return dates.

The contributions of ozone at each level to TOZ and its response to Cl_y and the linear trend is shown in Fig. 4. The models agree well in the climatological profile (upper left panel of Fig. 4). The Cl_y regression coefficients derived for each of the twelve CCMs

Full Screen / Esc

Printer-friendly Version

Interactive Discussion

(middle panel) also agree relatively well, with a negative response of ozone to Cl_y maximizing at 50 hPa. The response of mid-latitude ozone to Cl_y is stronger in the SH than in the NH, which is well known (Solomon, 1999). As outlined above, this higher sensitivity of ozone to Cl_y cannot explain the hemispheric asymmetry in return dates since Cl_y returns to 1980 levels at the same time in both hemispheres. The linear trend (upper right panel) shows significant inter-model differences in both amplitude and vertical structure. Most models show a positive trend in the troposphere; in the multi-model mean the trend is stronger in the NH than in the SH. The multi-model mean trends show a local maximum at ∼ 150 hPa. Above this level, trends in both hemisphere decrease with altitude up to ∼ 70 hPa. In the SH, about half of the models have a negative ozone trend between 70 and 50 hPa. Another local maximum, with positive trends in both hemispheres, is found at 30 hPa. Above 30 hPa, trends decrease towards zero and become hemispherically symmetric in the multi-model mean. The structure of the trends agrees well with the differences in cumulative ozone columns from the mid-20th to the end of the 21st century shown by Plummer et al. (2010). They used sensitivity simulations to attribute these trends almost fully to changes in GHG concentrations, thus validating our method of separating the effects of ODSs and GHGs through linear regression. We will show in Sect. 5 that the main processes responsible for the hemispheric differences in the vertical structure of ozone trends are changes in chemical reaction rates, that are in turn induced by GHG-induced changes in temperatures and dynamics.

4.2 Relation of hemispheric differences in the BDC to ozone return dates

The annual mean downward mass flux in each hemisphere, calculated from the residual circulation stream-function, is used as a measure of the strength of the BDC. The sum of the two hemispheric values is the total downward mass flux, equaling, in absolute value, the total upward mass flux, or tropical up-welling which is often used to quantify the strength of the BDC. The total downward mass flux in each hemisphere equals the meridional mass flux, which is responsible for transporting ozone from the

tropics to mid-latitudes. Trends in total downward mass flux in each hemisphere are shown in Fig. 5 (left) as a function of pressure. The trends are calculated using the same linear regression model as used to calculate the ozone trends. The mass flux increases in both hemispheres and in all models, consistent with the BDC strengthening as shown by Butchart et al. (2010). The multi-model mean trend in the NH is stronger than in the SH between 90 and 30 hPa (see Fig. 5, right). At 100 hPa, however, the trend is slightly stronger in the SH than in the NH.

If the hemispheric differences in the strengthening of the BDC were the cause of the hemispheric differences in ozone return dates, it would be expected that in models with a stronger hemispheric difference in the strengthening of the BDC, the hemispheric return dates would show greater separation. The relation between hemispheric differences in the strengthening of the BDC and hemispheric differences in ozone return dates is shown for the set of twelve CCMs in Fig. 6. The LSTR return date differences are plotted against the 70 hPa hemispheric differences in the mass flux trends (i.e. the 70 hPa values shown in Fig. 5 (left); 70 hPa is chosen since the hemispheric difference maximizes there). The return dates derived using method 1 are shown here, but results are similar for all three methods in that there is no statistically significant relationship between hemispheric differences in changes of the BDC and hemispheric differences in return dates. The T-test values are 0.6/0.6/0.04 for methods 1 to 3 (significance at the 80 % level is obtained at $T = 1.36$ for this sample size). Even when excluding the outlier seen on the lower right of the upper panel of Fig. 6 (with stronger circulation changes in the SH than NH), the correlation is not significant. The LMSTR return date differences are compared with the hemispheric differences in the mass flux trends at 100 hPa in the lower panel of Fig. 6. In the LMSTR a significant positive correlation at the 80 % significance level is found (and for one of the methods at the 90 % level). While the statistical significance is still rather weak, it provides evidence for some influence of hemispheric asymmetry in BDC changes being responsible for the hemispheric asymmetry in ozone return dates. Half of the models have a negative residual mass flux trend difference, i.e. the SH mass flux increases more than its NH counterpart (see

also right panel of Fig. 5). The return date differences for five of these models are, however, positive i.e. earlier return dates in the NH. This would not be possible if it was only the stronger transport by the BDC that controls the hemispheric difference in ozone return dates. Therefore, despite the (weak) correlation found between the BDC changes and the ozone return date differences, these results suggest that other processes play a significant role.

5 The role of transport and chemistry in driving ozone changes

The results presented in the previous section suggest that hemispheric differences in the strengthening of the BDC are unlikely to completely explain the hemispheric differences in ozone return dates as has been previously thought (WMO, 2011). In this section, two CCMs, E39CA and NIWA-SOCOL, that each incorporate a diagnostic to separate between chemical and transport induced changes in ozone (see Sect. 3.1) are used to investigate the processes leading to hemispheric asymmetric ozone trends.

5.1 Lowermost stratosphere and troposphere

The E39CA model is suitable for examining the ozone changes in the LMSTR since (i) the model behaves in a similar fashion to the multi-model mean in this region (see Figs. 4 and 5) and (ii) all relevant reaction cycles for this region are saved as output. Unfortunately, the tropospheric reaction cycles are not diagnosed in NIWA-SOCOL, hence only E39CA is used here.

The regression model including a Cl_y and linear trend term is applied to the time series of relative deviations of ozone from the 1960s (as shown exemplary in Fig. 1 for the time series at 45° S). In Fig. 7, the trend coefficient of the regression model applied to mid-latitude ozone (averaged over 45° to 60°) is shown as a function of height. The resulting units of the trends are percentage change in ozone per year.

Ozone increases linearly in the LMSTR and troposphere and the trend is stronger in the NH. The chemistry-transport diagnostic allows these trends to be attributed to trends in chemistry (blue lines) and trends in transport (red lines) as calculated using Eq. (2). The nonlinear term (6th term in Eq. 2) is also shown in Fig. 7 and it can be seen that this term becomes relevant only for large values of the chemistry and transport changes, e.g. around 250 hPa. The sum of the chemistry, transport and non-linear term is shown as the control trace (grey line). If this control line deviates from the net ozone trend, the imbalance term becomes important, and the results can not longer be easily interpreted. This occurs when the variability in the time series is large.

As shown in Fig. 7, in both hemispheres, between about 100 and 150 hPa, the positive trends in ozone result from positive trends in both transport and chemically-induced changes in ozone. Below 150 hPa, changes in chemistry drive a positive trend in ozone which maximizes at around 250 hPa. However, the chemically-induced posi-tive trend is largely offset by transport-induced negative ozone trends. The compen-sation of chemical effects by transport can be understood as follows: in the mean over the 1960s, at 250 hPa, production (of $0.32\,\mathrm{DU\,month^{-1}}$) is balanced by trans-port (of $-0.20\,\mathrm{DU\,month^{-1}}$) and by destruction (of $-0.12\,\mathrm{DU\,month^{-1}}$). Production in-creases to $0.53\,\mathrm{DU\,month^{-1}}$ in the 2040s, and this increase in production is mainly bal-anced by increased transport away from the source region (i.e. transport decreases to $-0.37\,\mathrm{DU\,month^{-1}}$), with the remainder balanced by destruction (decreasing to $-0.16\,\mathrm{DU\,month^{-1}}$). Thus, enhanced production leads to more ozone being available at any time step, and therefore more ozone can be transported away from this region leading to a negative effect on ozone values by transport. This effect becomes even more evident when employing an ozone origin diagnostic, as presented for E39CA in Garny et al. (2011) (see their Fig. 10).

Below 500 hPa in the NH and around 300 hPa in the SH, the transport term becomes positive, reinforcing the positive ozone trend. This suggests that ozone transport into this region dominates transport out of this region, as resulting from the stronger local production of ozone. It is most likely that it is ozone produced above these levels, and

transported downward, possibly together with horizontal transport, that leads to the overall positive contribution to ozone changes. Close to the surface, particularly in the NH, the increase in ozone due to chemistry again dominates. Again, transport changes offset the chemically-induced positive trend.

The hemispheric differences are highlighted in the lower-most panel in Fig. 7, showing that ozone trends are stronger in the NH compared to the SH, in particular in the upper troposphere. The stronger increase in ozone in the NH can be attributed to stronger chemically-induced ozone trends. The contribution from changes in transport largely offsets the contribution from changes in chemistry, but does not itself lead to asymmetric ozone trends in the LMSTR and troposphere. The induced asymmetry by chemistry is due to ozone production by NO_x, that increases more strongly in the NH, as will be shown in Sect. 6.1.

5.2 Lower stratosphere

Causes of ozone trends in the LSTR are investigated in more detail using the NIWA-SOCOL model. The ozone trends in this model behave similarly to the multi-model mean in the LSTR (see Fig. 4 and 5). E39CA, on the other hand, does not simulate the earlier return of NH ozone in the LSTR to 1980 levels, and the ozone trend profile is very different to most other models.

First, the latitudinal structure of trends in the LSTR partial ozone column from NIWA-SOCOL is shown in Fig. 8. Ozone trends are negative in the tropics, and positive at middle to high latitudes. Extratropical ozone trends are slightly stronger in the NH compared to the SH, consistent with earlier ozone return dates in the NH. The attribution of ozone trends shows that transport-induced changes lead to a decrease in ozone in the tropics and increases in the extratropics. The transport-induced trends change sign at about $45°$ N/S, motivating the choice of that latitude as equatorward boundary for our definition of mid-latitudes. The transport-induced ozone trends are consistent with an enhanced strength of the BDC. However, the stronger northern mid-latitude trends compared to southern mid-latitudes in NIWA-SOCOL cannot be

Ozone return dates

H. Garny et al.

◄◄   ►►

◄   ►

Back   Close

Full Screen / Esc

explained by differences in transport. Rather, transport changes induce stronger posi-
tive ozone trends in the southern mid-latitudes compared to the northern mid-latitudes.
The transport-induced trends in the SH are, partially, compensated by strong negative
trends induced by chemistry changes.

5   To elucidate this point further, profiles of mid-latitude (45–60° N/S) ozone trends,
attributed to changes in chemistry and transport within NIWA-SOCOL, are shown in
Fig. 9. Ozone trends at 100 hPa are positive in both hemispheres, decreasing with
height up to 70 hPa, where the trend in the SH is slightly negative. Above 70 hPa trends
increase with height and are positive throughout the LSTR.

10   Ozone trends induced by transport are positive at all levels in the LSTR in both
hemispheres, but maximize at 100 hPa and are close to zero above 20 hPa. Ozone
trends due to changes in chemistry are negative to around 40 to 30 hPa, and dominate
the positive ozone trend above 20 hPa in both hemispheres. The positive trend induced
by transport is again consistent with a strengthened BDC, and the decrease of the

15   effect with height is expected from the decreasing lifetime of ozone with height.

     The hemispheric differences in ozone trends, as shown in the lower panel of Fig. 9,
are positive throughout the LSTR, maximizing at 50 hPa. While changes in trans-
port are the main cause of relatively stronger NH trends below 80 hPa, chemistry-
induced trends are the major contributor above 80 hPa. Ozone trends integrated over

20   the lower stratospheric column are larger in the NH than the SH, primarily as a result
of chemistry-induced trends. On the other hand, transport changes lead to trends in-
tegrated over the LSTR to be larger in the SH compared to the NH (in agreement with
Fig. 8). These different trends are then reflected in the return dates, as summarized in
Fig. 15. Below 50 hPa, the sum of the attribution terms deviates from the actual ozone

25   trend differences, making the attribution less reliable. As discussed in Sect. 7, the dom-
inant role of chemistry-induced changes is robust against the uncertainties introduced
by the method. The causes for asymmetric ozone trends induced by chemistry in the
lower stratosphere are investigated in Sect. 6.2.

Ozone return dates

H. Garny et al.

Full Screen / Esc

6   Hemispheric differences in chemically induced ozone trends

6.1   Lowermost stratosphere and troposphere: enhancement in production by NO$_x$

In the LMSTR and upper troposphere, strong positive trends in ozone are induced by
5 changes in chemistry. Chemistry-induced trends are stronger in the NH than in the SH.
The contributions of individual reaction cycles to the chemically-induced increase in
ozone are averaged between 300 and 250 hPa and are shown in Fig. 10. The primary
contributor to ozone trends in this region, and the primary cause of hemispheric differ-
ences in ozone trends, is an increase in the production of ozone by NO$_x$, in particular
10 via the HO$_2$ + NO cycle (green bars in Fig. 10), which is significantly stronger in the NH
than in the SH. NO$_x$ concentrations increase in the troposphere due to stronger emis-
sions, and the increase is stronger in the NH, affecting tropospheric ozone (Lelieveld
and Dentener, 2000). Comparisons of NO$_x$ trends in the troposphere and LMSTR
between different CCMs showed clear discrepancies between individual models (not
15 shown), most likely as a result of differences in the prescribed emissions (or concentra-
tions) and differences in the way that tropospheric chemistry is simulated in the CCMs.
In E39CA, NO$_x$ trends ∼ 200 hPa are stronger compared to other models. Therefore,
the effect of enhanced production from the NO$_x$ cycles on ozone trends, as shown
here, might be overestimated. Consistently, ozone trends below 150 hPa are stronger
20 in E39CA compared to the multi-model mean (see Fig. 4). However, four of the models
show tropospheric ozone trends close to zero (most likely models that neglect tro-
pospheric chemistry), thus biasing the multi-model mean to lower values. In general,
tropospheric chemistry is often treated in a simplified manner in CCMs, introducing
uncertainty on the results shown here, as will be further discussed in Sect. 7.

Title Page

Abstract   Introduction

Conclusions   References

Tables   Figures

◄   ►

◄   ►

Back   Close

Full Screen / Esc

Printer-friendly Version

Interactive Discussion

6.2 Lower stratospheric chemistry

Changes in chemistry were shown to be the primary contributor to LSTR ozone trends and their hemispheric differences. The chemically-induced trend profiles from Fig. 9 are further divided into individual reaction cycles in Fig. 11.

Below 30 to 40 hPa, ozone trends induced by changes in chemistry are negative, caused primarily by changes in rates of ozone destruction by the HO_x cycles. The destruction rates of the HO_x cycle are affected by increasing CH_4 concentrations, with CH_4 being the primary source of stratospheric HO_x (Wuebbles and Hayhoe, 2002), and by changes in stratospheric water vapour (Stenke and Grewe, 2005). Changes in the rates of ozone destruction by the NO_x cycles cause an increase in ozone throughout the lower stratosphere, dominating the total chemistry-induced ozone trends above around 40 hPa. Changes in rates of ozone destruction by the NO_x cycles were analyzed in detail, based on the same NIWA-SOCOL simulation as used here, by Revell et al. (2012b). They showed that the decrease in ozone destruction by NO_x, despite an increase in N_2O, is caused by a decrease in the ratio of NO_x to N_2O and a reduction in the available atomic oxygen, both in turn largely due to GHG-induced stratospheric cooling.

The largest hemispheric differences in chemistry-induced ozone trends occur at 50 hPa, and are primarily due to ozone destruction by the (i) NO_x cycles and (ii) Cl_y cycles (see lower panel in Fig. 11). The increase in ozone caused by reduced ozone destruction by NO_x is stronger in the NH compared to the SH. The hemispheric differences in ozone trends due to changes in the Cl_y destruction cycles maximize at 70 hPa. While the changes caused by the Cl_y destruction cycles are slightly positive in the NH, they are negative in the SH at 70 hPa. The drivers of the trends in the destruction rates of the Cl_y and NO_x cycles are investigated below.

6.2.1 Changes in NO_x destruction rates

As discussed above, Revell et al. (2012b) showed that the effectiveness of N_2O in depleting ozone is determined by NO_x concentrations and by the availability in atomic oxygen. The former is strongly influenced by cooling of the stratosphere (Rosenfield and Douglass, 1998) and by changes in the strength of the BDC (Cook and Roscoe, 2012).

In Fig. 12, the vertical profile of linear trends in mid-latitude NO_x over the period 1960 to 2049 are shown, calculated in the same manner as the ozone trends, i.e. using a regression model taking an offset, Cl_y and a linear trend into account. Below 30 hPa, NO_x mixing ratios decrease slightly in the NH, whereas trends in the SH are close to zero. Above 30 hPa, trends are positive in both hemispheres and increase with height. Despite this increase in NO_x in both hemispheres above 30 hPa, ozone loss by the NO_x cycle decreases in this region. As explained by Revell et al. (2012b), this results from a decrease in the availability of atomic oxygen, which in turn is due to decreasing temperatures and to competition with other ozone destruction cycles, in particular the HO_x cycles.

The difference in the NO_x trends between the hemispheres, shown in the right panel, closely matches the difference in the NO_x-destruction induced ozone trends shown in Fig. 11; the stronger increase in NH ozone compared to the SH at 50 hPa is consistent with a slight decrease of NO_x in the NH and close to zero trend in NO_x in the SH. At 20 hPa, the sign of the hemispheric difference in NO_x trends is reversed (but uncertainties are large and trends are not statistically different), which is reflected in a slightly negative hemispheric difference in NO_x-destruction induced ozone trends (as shown in Fig. 11). At 10 hPa the NO_x trend in the SH is significantly stronger compared to the NH. This hemispheric difference in NO_x trends increases further up to 5 hPa (not shown). The stronger positive ozone trend, due to reduced NO_x-induced ozone destruction changes in the NH compared to the SH at 10 hPa (see Fig. 11), can again be explained by the asymmetric NO_x trends. Overall, the hemispheric differences in

the trends in ozone destruction rates by the NO_x cycle are consistent with hemispheric differences in NO_x trends.

6.2.2   Changes in Cl_y destruction rates

In the LSTR, the efficiency of homogenous Cl_y ozone destruction cycles is expected to decrease with decreasing temperatures (Rosenfield et al., 2002). As shown in Fig. 11, ozone trends due to changes in destruction rates by the Cl_y cycles are slightly positive throughout the lower stratosphere in the NH, consistent with decreasing temperatures. In the SH, on the other hand, a reduction in ozone resulting from an increase in the Cl_y destruction rates is found at 70 hPa.

The increase in ozone destruction rates cannot be due to changes in the abundance of Cl_y, since any changes in ozone congruent with Cl_y changes are included in the Cl_y regression coefficient. Therefore, the trend in ozone destruction rates must be caused by changes in the efficiency of a given amount of Cl_y to destroy ozone. The efficiency is determined by temperature, with lower temperatures slowing homogeneous reaction cycles. However, at very low temperatures, as those occurring in the Antarctic vortex, ozone can be depleted efficiently by heterogeneous chemistry. Hence, any expansion in space or time of the region where the conditions for heterogeneous chemistry occur, can cause an increase in the efficiency of the Cl_y ozone destruction cycles.

Trends in the rates of ozone destruction rates by the Cl_y cycles in southern mid-latitudes at 70 hPa are shown as a function of month in Fig. 13. Destruction rates increase (i.e. larger negative values) in mid-winter, and the trend maximizes in July. When disaggregating the destruction rates into individual reaction cycles, it can be seen that the largest contributor to the destruction rate increase in mid-winter is the ClO-dimer reaction cycle. Therefore, it is mostly heterogeneous chemistry that is responsible for the increased efficiency of ozone destruction. In mid-winter, the polar night prohibits heterogeneous ozone depletion south of 66.5° S for varying periods since sunlight is required for the photochemical reactions. Figure 14 shows the trend in temperatures over the southern middle to high latitudes at 70 hPa in July, where the increase in

Ozone return dates

H. Garny et al.

Printer-friendly Version

Interactive Discussion

heterogeneous ozone depletion maximizes. Temperature trends are negative over the polar region and maximize $\sim 60°$ S and 150° W. The pattern is suggestive of an intensification and shift of the polar vortex center away from the pole. Through this process, polar vortex air with low temperatures reaches latitudes equatorward of 60° S, where

5 sunlight is available in mid-winter, allowing for heterogeneous ozone depletion. This process can explain the negative trend in ozone at southern mid-latitudes at 70 hPa in NIWA-SOCOL.

7 Discussion

The implications of and uncertainties in the results presented in the last sections will be
10 discussed in the following. The results obtained with the attribution analysis (Sects. 5 and 6) are subject to two kinds of uncertainties: (1) uncertainties in the attribution method itself and (2) uncertainties in the model used for the attribution analysis. The latter refers to the question whether we can expect the processes identified in E39CA and NIWA-SOCOL to be of similar importance in other CCMs. To answer this question,
15 the attribution analysis would have to be applied to other models as well, which requires knowledge of the chemical loss and production rates. However, the comparison of NIWA-SOCOL and E39CA to the ensemble analysis of CCMs presented in the first half of the paper and to earlier studies allows us some estimations.

7.1 What is the role of transport for hemispheric asymmetric ozone trends?

20 Both the analysis of the relation of hemispheric differences in mid-latitude ozone return dates to asymmetric trends in the strength of the BDC and the attribution analysis to chemical and transport changes showed evidence that changes in transport of ozone plays a smaller role in explaining hemispherically asymmetric return dates as previously thought.

In the lower stratosphere, no significant correlation of ozone return date differences to asymmetric trends in the BDC strength is found across a set of twelve models. The attribution of ozone trends to transport and chemistry changes applied to NIWA-SOCOL showed that transport changes induce stronger positive ozone trends in the NH than SH at levels around 100 hPa. However, above 80 hPa, transport-induced ozone trends are stronger in the SH than in the NH. In the lower stratospheric column, chemically-induced changes dominate in driving an earlier return of ozone to 1980 values in the NH than in the SH, while transport-induced changes reduce this hemispheric difference (see Fig. 15). The negative effect on return date differences by transport can be understood as a compensation effect: chemically-induced increases in ozone cause more ozone to be available for the transport away from this region. Thus, the transport tendency decreases, even if air mass fluxes remain the same.

However, to obtain meaningful results with the attribution method, the changes in annual mean ozone tendencies needs to be small (i.e. the "imbalance" term negligible), so that the chemistry- and transport-induced changes together with the non-linear contribution equal the total change in ozone. As seen in Fig. 9, this is not the case below 50 hPa in the Southern Hemisphere, resulting in a discrepancy also in the hemispheric difference. These are the levels where transport-induced trends are of major importance; thus could we underestimate transport effects due to problems with the method in exactly the regions were transport seems to matter most? Let us assume that the difference between the estimated and actual ozone changes (i.e. the grey and black solid line in Fig. 9) would be entirely due to transport changes. Thus, we increase the hemispheric differences in transport-induced trends so that the estimated and actual ozone trends match. Then, the overall effect of transport changes on hemispheric differences in ozone trends in the lower stratospheric column would be slightly positive instead of negative. However, chemistry-induced asymmetry in return dates in the lower stratospheric column would still dominate over the transport-induced asymmetry by a factor of 10. Thus, the conclusion that chemistry is the dominant factor in driving hemispheric

⏮ | ⏭

◀ | ▶

Back | Close

Full Screen / Esc

Printer-friendly Version

Interactive Discussion

asymmetries in lower stratospheric ozone trends is insensitive to the uncertainties in the attribution method.

Concerning uncertainties stemming from the choice of the model, NIWA-SOCOL simulates increases in the strength of the mass fluxes that are above average (Fig. 5). The hemispheric differences in the 70 hPa mass fluxes are slightly larger compared to most models (Fig. 6). Thus, if transport were to play an important role in driving asymmetric ozone trends, it should be apparent in the NIWA-SOCOL model.

In the lowermost stratosphere, we found a weak correlation between the hemispheric differences in the BDC changes at 100 hPa and the differences in return dates for the ensemble of twelve CCMs. A closer investigation with E39CA showed that the positive trends in this region are in large parts caused by chemically induced changes, which are stronger in the NH and thus introduces hemispheric differences. The attribution method works reasonably well in this region for E39CA, as seen from the approximate agreement of the ozone changes and control line (black dashed) in Fig. 7. The model E39CA simulates stronger than average strengthening of the downward mass flux at 100 hPa (Fig. 5), but hemispheric differences here are small (Fig. 6). A group of four models simulate stronger hemispheric differences in the mass flux trends, and larger asymmetries in the return dates. Thus, for this group of models, transport changes might play a larger role. Another group of five models simulates two to five years earlier return dates of LMSTR ozone in the NH, but stronger mass flux increases in the SH than to the NH. For this group of models, the correlation between return date difference and asymmetric circulation changes apparently breaks down. The combination of stronger BDC changes in the SH but earlier return in the NH can only be explained if other processes than transport induce additional hemispheric asymmetric trends. Thus, it appears likely that at least in this group of models, chemistry-induced changes play the leading role in introducing the hemispheric differences.

Overall the results suggest that the hemispheric differences in ozone trends, and thus return dates in the lowermost stratosphere are caused by a combination of (i) enhanced ozone production by increasing NO_x concentrations, which is stronger in the

Ozone return dates

H. Garny et al.

NH, and (ii) hemispheric different transport changes, due to the hemispheric asymmetric BDC trends. The relative importance of the mechanisms probably varies from model to model.

7.2 What is the relevance of the identified chemical processes?

7.2.1 Lowermost stratosphere and troposphere: NO_x-related production

In the lowermost stratosphere and upper troposphere, analysis of the E39CA model reveals an important contribution to positive ozone trends from ozone production by the NO_x production cycles. Due to stronger increases in NO_x concentrations in the NH, the production increase is larger there compared to the SH, and thus leads to asymmetric ozone trends. Even though the absolute amount of NO_x seems to be simulated well in E39CA (as indicated by a brief comparison to a tropospheric chemistry model and to observations, not shown), the trends are larger compared to other CCMs. Thus, the effect of NO_x-related ozone production might be less relevant in other CCMs. In addition, despite E39CA had been used to examine variability in tropospheric ozone, the model incorporates only background tropospheric chemistry, which limits the capabilities to accurately simulate trends (Grewe, 2007). However, the increase in the tropospheric ozone burden from 2000 to 2030 of around 10 % in E39CA compares reasonably well with the estimates of an ensemble of models focused on tropospheric chemistry of 6 to 15 %, depending on the scenario, given by Stevenson et al. (2006).

The comparison of NO_x concentrations in the troposphere among the ensemble of CCMs (not shown here) reveals large discrepancies of simulated values between the models. The large spread is mostly a result of differences in prescribed NO_x emissions (or concentrations), and of differences in the treatment of tropospheric chemistry. Since the CCMs are focused on stratospheric chemistry, the tropospheric chemistry is often simulated in a simplified manner.

7.2.2 Lower stratosphere: NO_x destruction cycles

The hemispheric differences in the decrease of ozone destruction by the NO_x cycles are found to be controlled by hemispheric differences in the trends in NO_x concentrations. The detailed analysis of the causes for the hemispheric differences in NO_x trends are beyond the scope of this study. From previous studies, it is known that trends in stratospheric NO_x concentrations are influenced by the speed of the BDC (Plummer et al., 2010; Cook and Roscoe, 2012). Thus, one possible explanation of the hemispheric differences in NO_x trends could be a feedback of changes in the circulation on the efficiency of the production of NO_x. As shown by Cook and Roscoe (2012) in a simplified model approach, an increase in the BDC causes a decrease in the formation of NO_x (since the time available for photolysis decreases, and this effect dominates over the enhanced influx of the tropospheric source gas N_2O). Climatologically, the BDC is stronger in the NH compared to the SH, and in agreement with the work of Cook and Roscoe (2012), climatological NO_x concentrations in NIWA-SOCOL are higher in the SH than in the NH (not shown). A stronger increase in the strength of the BDC in the middle stratosphere of the NH could thus explain weaker positive NO_x trends in the NH compared to the SH.

Compared to other models, trends in NO_x concentrations at 10 hPa in NIWA-SOCOL are of similar magnitude. In addition, most models show a stronger NO_x trend in the SH than in the NH (not shown), indicating that the hemispheric asymmetric changes in NO_x concentrations can be a relevant factor in determining the hemispheric different ozone trends and thus return dates.

As opposed to most other models, E39CA simulates a slightly earlier return of lower stratospheric ozone in the SH than in the NH (see Fig. 6), and ozone trends are negative above 30 hPa in contrast to the remaining group of CCMs analyzed here (see Fig. 4). What are the causes for the different behavior of E39CA, and can we learn something from that on the necessary ingredients for capturing the return date difference in models? The attribution analysis of lower stratospheric ozone from E39CA is

given in Appendix A. It is shown that in E39CA the chemically-induced ozone trends are negative throughout the lower stratosphere. The hemispheric difference in chemically-induced ozone trends, which was found to be of major importance in NIWA-SOCOL, is much smaller. The negative chemically-induced ozone trends can be largely at-
5 tributed to the NO_x destruction cycles. The increase in destruction rates by the NO_x cycles is in turn caused by strong positive trends in NO_x (exceeding the NO_x trends in NIWA-SOCOL almost by a factor of 4), and the trends are identical in the two hemi-spheres, explaining the lack of chemically-induced hemispheric differences in ozone trends. Since in E39CA, NO_y (= $NO_x + HNO_3$) concentrations are prescribed at the up-
10 per level at 10 hPa, and concentrations are assumed to increase with the same rate as N_2O, any influence of changes in temperature and dynamics on NO_y production is not accounted for. Thus, the impact of dynamical and temperature changes on NO_x concentrations can be concluded to be crucial for both the response of ozone to N_2O changes, in agreement with earlier studies (Plummer et al., 2010; Revell et al., 2012b),
15 and furthermore on the hemispheric asymmetry of ozone trends, as the results of this study suggest.

7.2.3 Lower stratosphere: Cl_y destruction cycles

Changes in the efficiency of Cl_y to deplete ozone is found to be one of the causes for hemispheric asymmetries in ozone trends. Enhanced efficiencies are found in the SH,
20 where an expansion or shift of the polar vortex provides the conditions for heteroge-neous ozone depletion in mid-winter north of 60° S. This effect was noted earlier for southern polar ozone for example by Plummer et al. (2010), who found a non-linearity of the response of ozone to ODSs in the Antarctic lower stratosphere under changing GHG concentrations. Similarly, Revell et al. (2012a) reported an increase of Antarctic
25 lower stratospheric ozone in a scenario with lower GHG concentration increases as compared to the standard REF-B2 simulation. The results presented here suggest that the effect of GHG-induced cooling on homogenous ozone depletion is of importance in particular for the evolution of ozone in the mid-latitudes.

Title Page

Abstract | Introduction

Conclusions | References

Tables | Figures

◀ | ▶

◀ | ▶

Back | Close

Full Screen / Esc

Printer-friendly Version

Interactive Discussion

The trend analysis of the ensemble of CCMs reveals negative trends in SH mid-latitude ozone around 70 to 50 hPa in about half of the models, indicating that the effect of an increasing efficiency of destruction by Cl_y chemistry is of importance not only in NIWA-SOCOL. The strength of this effect will depend strongly on the pattern of dynamical changes, in particular in the location and timing of the Antarctic vortex, simulated in each individual model. Thus, the variety of the simulated changes in the polar vortex likely accounts at least in parts for the spread in the ozone trends and thus ozone return dates simulated by the different models.

8 Conclusions

The detailed investigation of mid-latitude return dates of TOZ to 1980 values from an ensemble of twelve CCMVal models, with particular focus on the hemispheric differences, confirmed recent studies (e.g. WMO, 2011) in that the earlier return date in the northern mid-latitudes compared to the southern mid-latitudes is a robust result. However, we found that there are large differences between individual models, with hemispheric return date differences ranging from about 0 to 30 yr for TOZ. The method used to estimate the return dates can cause deviations of the results for the hemispheric difference in return dates of up to 5 to 10 yr for individual models. Although results for individual models slightly depend on the applied method, the multi-model mean is barely affected by the method used.

As summarized in Fig. 15, the hemispheric differences in total column return dates are due to differences in ozone trends in the lower stratosphere and lowermost stratosphere/troposphere. Based on the models NIWA-SOCOL and E39CA, processes driving hemispheric differences in return dates are identified. The key result of this study is that changes in chemical production and loss play the major role in driving hemispheric differences in ozone return dates. The statement in WMO (2011), that the "more pronounced strengthening of the poleward transport of ozone" is the cause of the earlier return of ozone in the NH could not be confirmed in the present study. The chemically-

Ozone return dates

H. Garny et al.

Title Page

Abstract	Introduction
Conclusions	References
Tables	Figures

Back | Close

Full Screen / Esc

Printer-friendly Version

Interactive Discussion

induced changes identified in the lower stratosphere are, however, likely indirectly influenced by asymmetric BDC changes, that influence transport of ozone precursors, the rate at which these are produced by photolysis and temperatures that affect reaction rates. In particular, the main chemical processes identified here are the relatively less efficient destruction of ozone by NO_x chemistry in the NH, caused by likely dynamical influences on NO_x concentrations, and the relatively more efficient destruction of ozone by Cl_y in the SH due to an expansion of the polar vortex into mid-latitudes in mid-winter.

Furthermore, ozone trends in the lowermost stratosphere and troposphere are found to contribute significantly to the hemispheric asymmetry in TOZ return dates. Enhanced production of ozone due to increasing NO_x emissions are identified to introduce the hemispheric asymmetries in ozone trends. Since tropospheric chemistry is treated in a simplified manner in the CCMs used here, studies with improved representations of tropospheric chemistry will be necessary to validate this result. Overall it can be concluded that the uncertainties introduced by the treatment of tropospheric chemistry and ozone precursor emissions are not negligible for the correct simulation of the temporal development of TOZ.

Appendix A

Lower stratospheric trends in E39CA

E39CA is identified as outlier in terms of ozone trends in the lower stratosphere. However, the attribution analysis can help to understand the causes for the different behavior of E39CA, which potentially can reveal important factors determining the trends in other models, and that are lacking here. The attribution of ozone trends in the lower stratosphere to transport- and chemically-induced changes is shown in Fig. A1, and the further attribution to chemical reaction cycles in Fig. A2.

Transport-induced trends in ozone in the LSTR in E39CA have a similar vertical structure compared to NIWA-SOCOL, with strongest positive trends close to 100 hPa. However, in E39CA transport-induced trends are stronger in the SH than in the NH, thus inducing the overall larger trends and earlier return of ozone to 1980 levels in the SH. The chemically-induced trends behave quite different to NIWA-SOCOL: trends are negative at all levels above 100 hPa, thus lacking the transition to positive chemically-induced trends induced by chemistry seen in NIWA-SOCOL. The negative chemically-induced trends can be explained by negative trends induced by changes in the destruction rates of the NO_x cycles (see Fig. A2). In Fig. A3, trends in NO_x concentrations in E39CA are shown to be almost by a factor of 4 larger compared to the trends in NIWA-SOCOL. Furthermore, the lack of hemispheric differences in NO_x trends explains the weaker hemispheric asymmetries induced by chemistry in the lower stratosphere in E39CA.

References

Austin, J., Scinocca, J., Plummer, D., Oman, L., Waugh, D., Akiyoshi, H., Bekki, S., Braesicke, P., Butchart, N., Chipperfield, M., Cugnet, D., Dameris, M., Dhomse, S., Eyring, V., Frith, S., Garcia, R., Garny, H., Gettelman, A., Hardiman, S. C., Kinnison, D., Lamar-que, J., Mancini, E., Marchand, M., Michou, M., Morgenstern, O., Nakamura, T., Pawson, S.,

Pitari, G., Pyle, J., Rozanov, E., Shepherd, T., Shibata, K., Stolarski, R., Teyssedre, H., Wilson, R., and Yamashita, Y.: The decline and recovery of total column ozone using a multimodel time series analysis, J. Geophys. Res., 115, D00M10, doi:10.1029/2010JD013857, 2010. 32827, 32828, 32837, 32840

5 Butchart, N., Cionni, I., Eyring, V., Waugh, D. W., Akiyoshi, H., Austin, J., Bruehl, C., Chipperfield, M. P., Cordero, E., Dameris, M., Deckert, R., Frith, S. M., Garcia, R. R., Gettelman, A., Giorgetta, M. A., Kinnison, D. E., Li, F., Manzini, E., McLandress, C., Pawson, S., Pitari, G., Rozanov, E., Sassi, F., Shepherd, T. G., Shibata, K., and Tian, W.: Chemistry-climate model simulations of twenty-first century stratospheric climate and circulation changes, J. Climate,
10 23, 5349–5374, 2010. 32828, 32842

Cook, P. A. and Roscoe, H. K.: Changes in reactive stratospheric gases due to a chnge in Brewer–Dobson circulation: results from a simple model, Atmos. Sci. Lett., 13, 49–54, 2012. 32828, 32849, 32855

Dameris, M., Grewe, V., Ponater, M., Deckert, R., Eyring, V., Mager, F., Matthes, S., Schnadt, C.,
15 Stenke, A., Steil, B., Brühl, C., and Giorgetta, M. A.: Long-term changes and variability in a transient simulation with a chemistry-climate model employing realistic forcing, Atmos. Chem. Phys., 5, 2121–2145, doi:10.5194/acp-5-2121-2005, 2005. 32830

Egorova, T., Rozanov, E., Zubov, V., and Karol, I.: Model for investigating ozone trends (MEZON), Izv. Atmos. Ocean. Phys., 39, 277–292, 2003. 32829

20 Eyring, V., Chipperfield, M., Giorgetta, M., Kinnison, D. E., Manzini, E., Matthes, K., Newman, P., Pawson, S., Shepherd, T., and Waugh, D.: Overview of the new CCMVal reference and sensitivity simulations in support of upcoming ozone and climate assessments and planned SPARC CCMVal, SPARC Newsletter, 30, 20–26, 2008. 32829

Eyring, V., Cionni, I., Bodeker, G. E., Charlton-Perez, A. J., Kinnison, D. E., Scinocca, J. F.,
25 Waugh, D. W., Akiyoshi, H., Bekki, S., Chipperfield, M. P., Dameris, M., Dhomse, S., Frith, S. M., Garny, H., Gettelman, A., Kubin, A., Langematz, U., Mancini, E., Marchand, M., Nakamura, T., Oman, L. D., Pawson, S., Pitari, G., Plummer, D. A., Rozanov, E., Shepherd, T. G., Shibata, K., Tian, W., Braesicke, P., Hardiman, S. C., Lamarque, J. F., Morgenstern, O., Pyle, J. A., Smale, D., and Yamashita, Y.: Multi-model assessment of strato-
30 spheric ozone return dates and ozone recovery in CCMVal-2 models, Atmos. Chem. Phys., 10, 9451–9472, doi:10.5194/acp-10-9451-2010, 2010. 32827, 32828, 32837, 32840

Garny, H., Dameris, M., and Stenke, A.: Impact of prescribed SSTs on climatologies and long-term trends in CCM simulations, Atmos. Chem. Phys., 9, 6017–6031, doi:10.5194/acp-9-6017-2009, 2009. 32831

Garny, H., Grewe, V., Dameris, M., Bodeker, G. E., and Stenke, A.: Attribution of ozone changes to dynamical and chemical processes in CCMs and CTMs, Geosci. Model Dev., 4, 271–286, doi:10.5194/gmd-4-271-2011, 2011. 32832, 32833, 32844

5 Grewe, V.: Impact of climate variability on tropospheric ozone, Sci. Total Environ., 374, 167–181, 2007. 32854

Hein, R., Dameris, M., Schnadt, C., Land, C., Grewe, V., Köhler, I., Ponater, M., Sausen, R., B. Steil, B., Landgraf, J., and Brühl, C.: Results of an interactively coupled atmospheric chemistry – general circulation model: Comparison with observations, Ann. Geophys., 19, 435–457, doi:10.5194/angeo-19-435-2001, 2001. 32830

10 Land, C., Feichter, J., and Sausen, R.: Impact of vertical resolution on the transport of passive tracers in the ECHAM4 model, Tellus B, 54, 344–360, 2002. 32831

Lelieveld, J. and Dentener, F. J.: What controls tropospheric ozone?, J. Geophys. Res., 105, 3531–3551, 2000. 32847

15 Montzka, S. A., Butler, J. H., Elkins, J. W., Thompson, T. M., Clarke, A. D., and Lock, L. T.: Present and future trends in the atmospheric burden of ozone-depleting halogens, Nature, 398, 690–694, 1999. 32827

Morgenstern, O., Giorgetta, M. A., Shibata, K., Eyring, V., Waugh, D. W., Shepherd, T. G., Akiyoshi, H., Austin, J., Baumgaertner, A. J. G., Bekki, S., Braesicke, P., Brühl, C., Chipper-
20 field, M. P., Cugnet, D., Dameris, M., Dhomse, S., Frith, S. M., Garny, H., Gettelman, A., Hardiman, S. C., Hegglin, M. I., Jöckel, P., Kinnison, D. E., Lamarque, J., Mancini, E., Manzini, E., Marchand, M., Michou, M., Nakamura, T., Nielsen, J. E., Olivié, D., Pitari, G., Plummer, D. A., Rozanov, E., Scinocca, J. F., Smale, D., Teyssèdre, H., Toohey, M., Tian, W., and Yamashita, Y.: Review of the formulation of present-generation stratospheric
25 chemistry-climate models and associated external forcings, J. Geophys. Res., 115, D00M02, doi:10.1029/2009JD013728, 2010. 32829, 32830

Oman, L. D., Plummer, D., Waugh, D., Austin, J., Scinocca, J., Douglass, A., Salawitch, R., Canty, T., Akiyoshi, H., Bekki, S., Braesicke, P., Butchart, N., Chipperfield, M., Cugnet, D., Dhomse, S., Eyring, V., Frith, S., Hardiman, S., Kinnison, D., Lamarque, J., Mancini, E.,
30 Marchand, M., Michou, M., Morgenstern, O., Nakamura, T., Nielsen, J., Olivie, D., Pitari, G., Pyle, J., Rozanov, E., Shepherd, T., Shibata, K., Stolarski, R., Teyssedre, H., Tian, W., and

Ozone return dates

H. Garny et al.

Title Page

Abstract | Introduction

Conclusions | References

Tables | Figures

◄ | ►

◄ | ►

Back | Close

Full Screen / Esc

Printer-friendly Version

Interactive Discussion

Yamashita, Y.: Multi-model assessment of the factors driving stratospheric ozone evolution over the 21st century, J. Geophys. Res., 115, D24306, doi:10.1029/2010JD014362, 2010. 32827, 32840

Plummer, D. A., Scinocca, J. F., Shepherd, T. G., Reader, M. C., and Jonsson, A. I.: Quantifying the contributions to stratospheric ozone changes from ozone depleting substances and greenhouse gases, Atmos. Chem. Phys., 10, 8803–8820, doi:10.5194/acp-10-8803-2010, 2010. 32828, 32841, 32855, 32856

Portmann, R. W. and Solomon, S.: Indirect radiative forcing of the ozone layer during the 21st century, Geophys. Res. Lett., 34, L02813, doi:10.1029/2006GL028252, 2007. 32827

Reithmeier, C. and Sausen, R.: ATTILA: atmospheric tracer transport in a Lagrangian model, Tellus B, 54, 278–299, 2002. 32830

Revell, L. E., Bodeker, G. E., Huck, P. E., and Williamson, B. E.: Impacts of the production and consumption of biofuels on stratospheric ozone, Geophys. Res. Lett., 39, L10804, doi:10.1029/2012GL051546, 2012a. 32856

Revell, L. E., Bodeker, G. E., Smale, D., Lehmann, R., Huck, P. E., Williamson, B. E., Rozanov, E., and Struthers, H.: The effectiveness of N_2O in depleting stratospheric ozone, Geophys. Res. Lett., 39, L15806, doi:10.1029/2012GL052143, 2012b. 32828, 32830, 32848, 32849, 32856

Rosenfield, J. and Douglass, A.: (1998), Doubled CO_2 effects on NO_y in a coupled 2D model, Geophys. Res. Lett., 25, 4381–4384, 1998. 32849

Rosenfield, J. E., Douglass, A. R., and Considine, D.: The impact of increasing carbon dioxide on ozone recovery, J. Geophys. Res., 107, D64049, doi:10.1029/2001JD000824, 2002. 32850

Schraner, M., Rozanov, E., Schnadt Poberaj, C., Kenzelmann, P., Fischer, A. M., Zubov, V., Luo, B. P., Hoyle, C. R., Egorova, T., Fueglistaler, S., Brönnimann, S., Schmutz, W., and Peter, T.: Technical Note: Chemistry-climate model SOCOL: version 2.0 with improved transport and chemistry/microphysics schemes, Atmos. Chem. Phys., 8, 5957–5974, doi:10.5194/acp-8-5957-2008, 2008. 32829

Scinocca, J. F., Stephenson, D. B., Bailey, T. C., and Austin, J.: Estimates of past and future ozone trends from multimodel simulations using a flexible smoothing spline methodology, J. Geophys. Res., 115, D00M12, doi:10.1029/2009JD013622, 2010. 32834

Solomon, S.: Stratospheric ozone depletion: A review of concepts and history, Rev. Geophys., 37, 275–316, 1999. 32841

Ozone return dates

H. Garny et al.

Title Page

Abstract	Introduction
Conclusions	References
Tables	Figures

◄ | ►|

◄ | ►

Back | Close

Full Screen / Esc

Printer-friendly Version

Interactive Discussion

SPARC-CCMVal: SPARC Report on the Evaluation of Chemistry-Climate Models, edited by: Eyring, V., Shepherd, T. G., and Waugh, D. W., SPARC Report No. 5, Tech. Rep., WCRP-132, WMO/TD-No. 1526, available at: http://www.atmosp.physics.utoronto.ca/SPARC, 2010. 32827, 32829, 32835, 32837

Steil, B., Dameris, M., Brühl, C., Crutzen, P. J., Grewe, V., Ponater, M., and Sausen, R.: Development of a chemistry module for GCMs: first results of a multiannual integration, Ann. Geophys., 16, 205–228, doi:10.1007/s00585-998-0205-8, 1998. 32831

Stenke, A. and Grewe, V.: Simulation of stratospheric water vapor trends: impact on stratospheric ozone chemistry, Atmos. Chem. Phys., 5, 1257–1272, doi:10.5194/acp-5-1257-2005, 2005. 32848

Stenke, A., Dameris, M., Grewe, V., and Garny, H.: Implications of Lagrangian transport for simulations with a coupled chemistry-climate model, Atmos. Chem. Phys., 9, 5489–5504, doi:10.5194/acp-9-5489-2009, 2009. 32830, 32831

Stevenson, D. S., Dentener, F. J., Schultz, M. G., Ellingsen, K., van Noije, T. P. C., Wild, O., Zeng, G., Amann, M., Atherton, C. S., Bell, N., Bergmann, D. J., Bey, I., Butler, T., Cofala, J., Collins, W. J., Derwent, R. G., Doherty, R. M., Drevet, J., Eskes, H. J., Fiore, A. M., Gauss, M., Hauglustaine, D. A., Horowitz, L. W., Isaksen, I. S. A., Krol, M. C., Lamarque, J., Lawrence, M. G., Montanaro, V., Müller, J., Pitari, G., Prather, M. J., Pyle, J. A., Rast, S., Rodriguez, J. M., Sanderson, M. G., Savage, N. H., Shindell, D. T., Strahan, S. E., Sudo, K., and Szopa, S.: Multimodel ensemble simulations of present-day and near-future tropospheric ozone, J. Geophys. Res., 111, D08301, doi:10.1029/2005JD006338, 2006. 32854

WMO: Scientific Assessment of Ozone Depletion: 2010, Tech. rep., Global Ozone Research and Monitoring Project-Report No. 52, Geneva, Switzerland, 516 pp., 2011. 32826, 32828, 32834, 32838, 32839, 32843, 32857

Wuebbles, D. J. and Hayhoe, K.: Atmospheric methane and global change, Earth-Sci. Rev., 57, 177–210, 2002. 32848

Title Page

Abstract | Introduction

Conclusions | References

Tables | Figures

◀ | ▶

◀ | ▶

Back | Close

Full Screen / Esc

Printer-friendly Version

Interactive Discussion
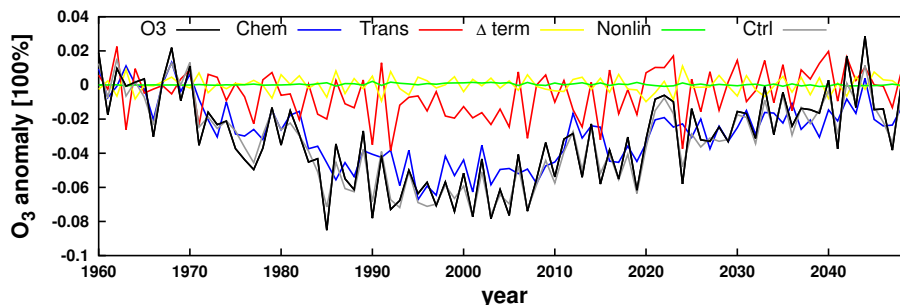
Fig. 1. Demonstration of ozone attribution method: time series of zonal mean lower strato-spheric partial column ozone at 45° S relative to the mean 1960–69 (black solid line) as simu-lated by E39CA, together with changes induced by transport (red), changes induced by chem-istry (blue), the imbalance term (yellow), the non-linear term (green) and the sum of these four terms (control line, grey).
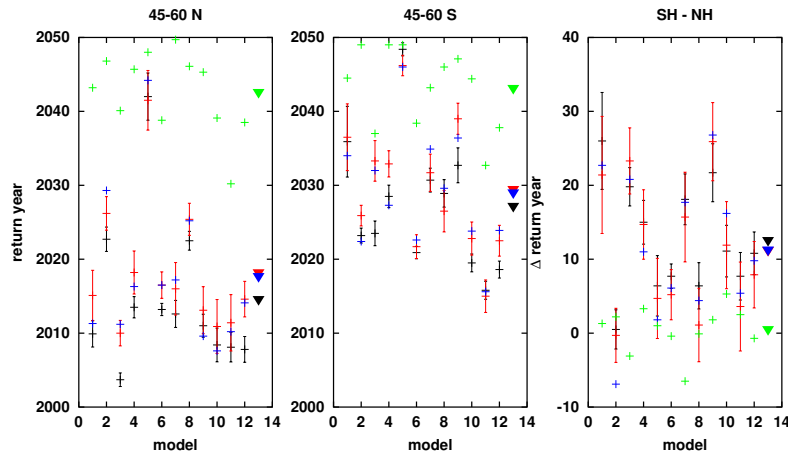
Fig. 2. Return dates to 1980 values of mid-latitude total column ozone for twelve different CCMs using a simple regression (black, with uncertainties), using advanced regression (red, with uncertainties) and smoothing (blue) together with 50 hPa Cl_y return dates (green). Triangles on the right are the multi-model mean. Left panel: NH mid-latitudes (45–60° N), middle: SH mid-latitudes (45–60° S) and right: SH – NH.
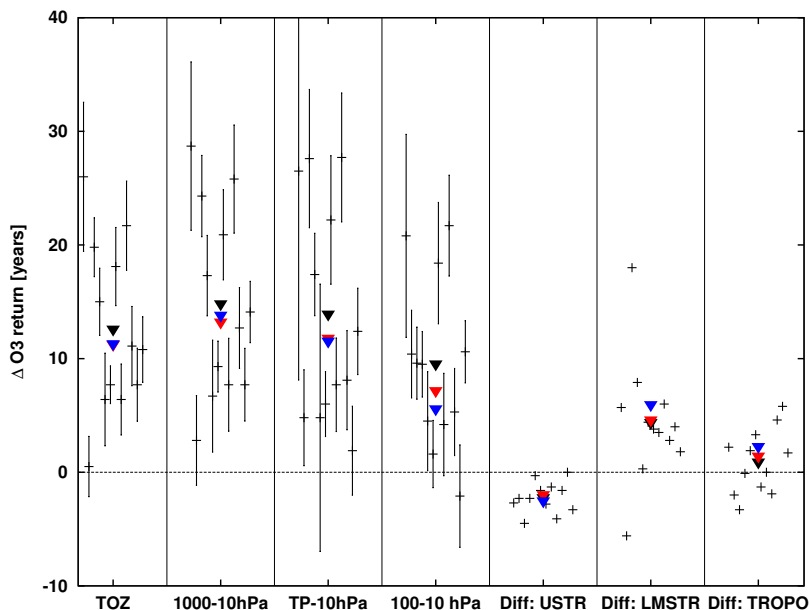
Fig. 3. Hemispheric difference ((45° to 60° S) – (45° to 60° N)) in return dates of ozone to 1980 values for twelve different models (back crosses with uncertainty bars) and the multi-model mean (triangle) for total column ozone (left), and partial column ozone from the surface to 10 hPa (second from left), from the tropopause to 10 hPa (third from left) and 100 hPa to 10 hPa (fourth from left). Furthermore the impact on hemispheric differences in return dates from the upper stratosphere (third from right; difference of the TOZ to the 1000–10 hPa return date differences), from the lowermost stratosphere (second from right; difference of the tropopause–10 hPa to the 100–10 hPa return date differences) and from the tropopause (right; difference of the 1000–10 hPa to the tropopause–10 hPa return date differences). The results for method 1 are shown in black, and the multi-model means are shown as well for method 2 (red) and 3 (blue).

Ozone return dates

H. Garny et al.

Title Page

Abstract | Introduction

Conclusions | References

Tables | Figures

◄ | ►

◄ | ►

Back | Close

Full Screen / Esc

Printer-friendly Version

Interactive Discussion
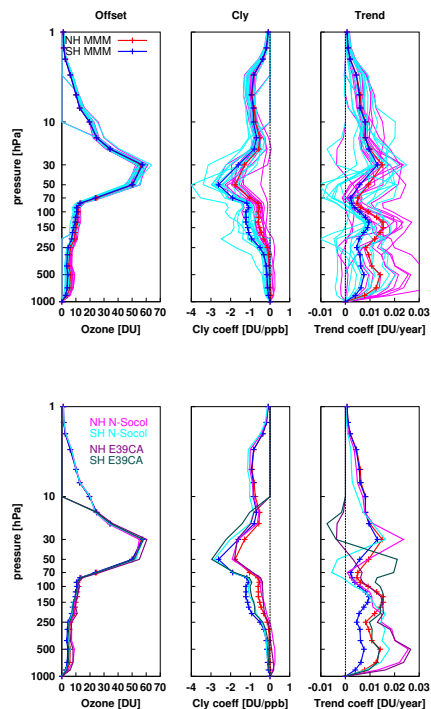
Fig. 4. Profiles of annual mean contribution to TOZ at each level (in DU $1 DU = 2.69 \times 10^{16}$ molecules cm^{-2}; the sum of the values at each pressure level equals TOZ). The climatology (left), Cl$_y$ regression coefficient (middle) and trend coefficient (right) over the period 1960 to 2049 is shown for the multi-model mean of the NH (red) and the SH (blue) mid-latitudes. Individual models are shown in pink for the NH and light blue for the SH. The lower panel repeats the multi-model mean from above, and highlights the models NIWA-SOCOL (light colors) and E39CA (dark colors).

Title Page

Abstract | Introduction

Conclusions | References

Tables | Figures

◀ | ▶

◀ | ▶

Back | Close

Full Screen / Esc

Printer-friendly Version

Interactive Discussion
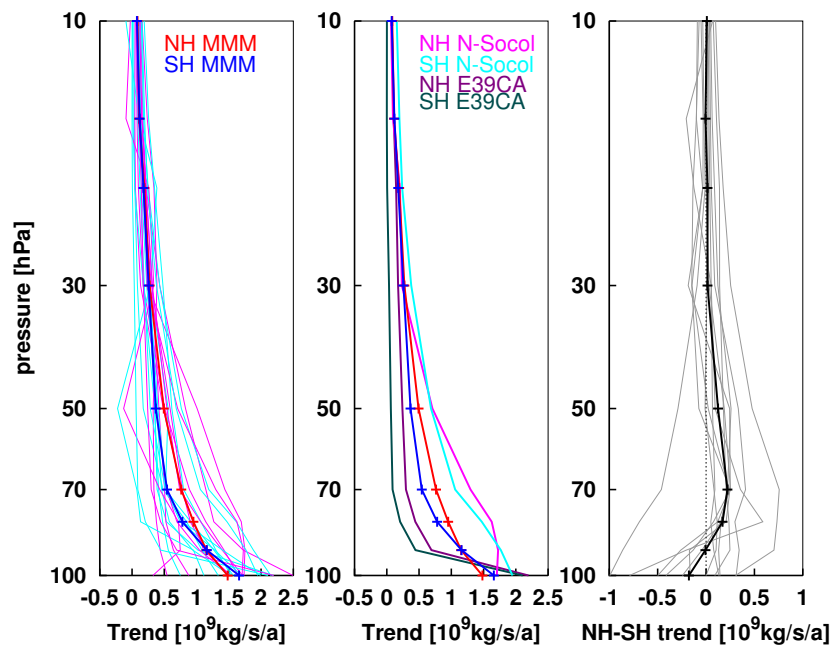
Fig. 5. Profiles of trends in the annual mean residual circulation total downward massflux in each hemisphere over 1960 to 2049, individual models and multi-model mean color-coded as in Fig. 4. Right: difference NH – SH downward mass fluxes for the multi-model mean (black) and individual models (grey lines).
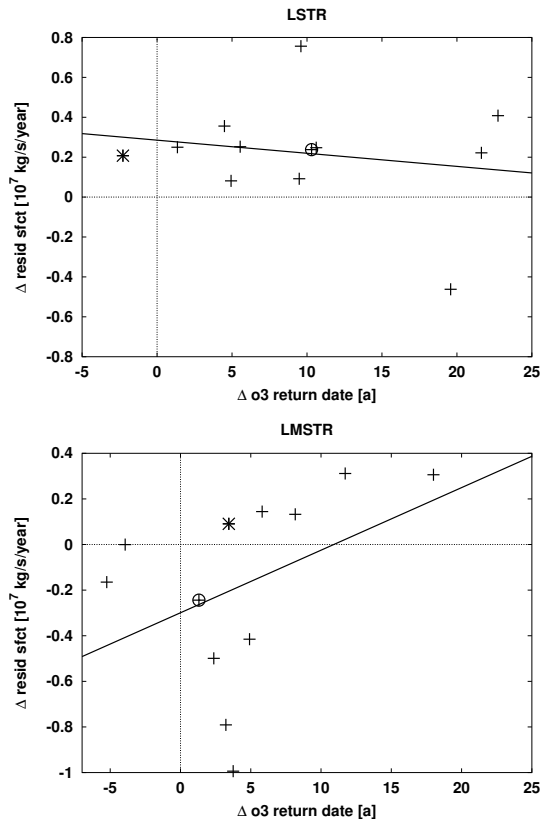
Fig. 6. Top: hemispheric differences (NH – SH) in the strength of trends in the residual circulation mass flux at 70 hPa plotted against hemispheric differences (SH – NH mid-latitudes) in lower stratospheric return dates for twelve different models (crosses) and their linear fit (line). Bottom: as left but hemispheric differences in 100 hPa residual circulation mass flux trends against lowermost stratospheric return date differences. The model marked with a circle is NIWA-SOCOL, the model marked with a star is E39CA.
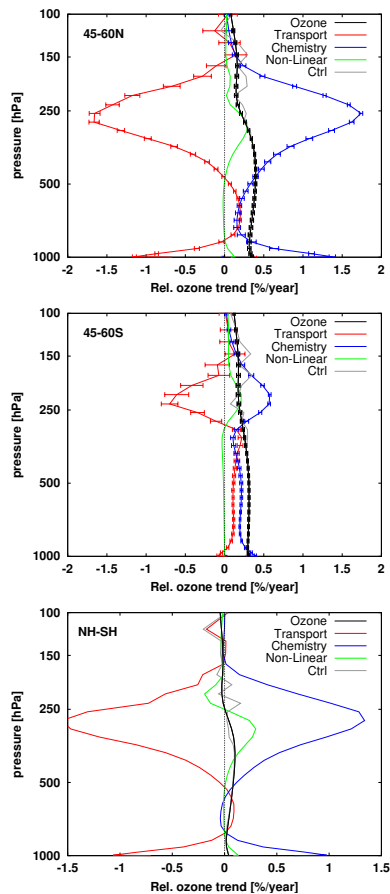
Fig. 7. Profile of relative trends in ozone (in units of % per year) from E39CA over the period 1960 to 2049 (black). Chemistry- and transport-induced trends in ozone are shown in blue and red, the nonlinear term in green and the sum of these three in grey ("Ctrl"). Top: 45° to 60° N, middle: 45° to 60° S, bottom: NH – SH.

Ozone return dates

H. Garny et al.

Title Page

Abstract | Introduction

Conclusions | References

Tables | Figures

◀ | ▶

◀ | ▶

Back | Close

Full Screen / Esc

Printer-friendly Version

Interactive Discussion
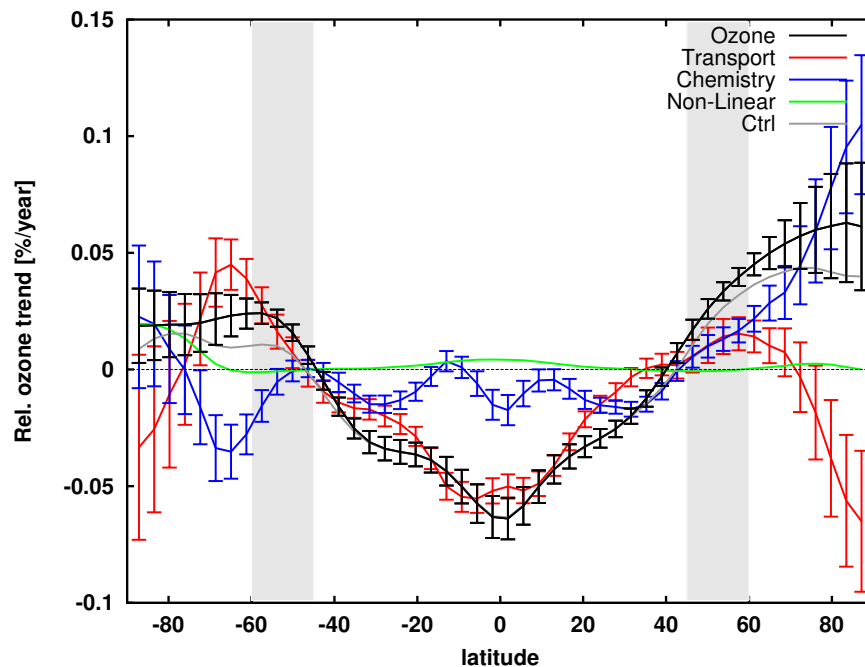
Fig. 8. Trend regression coefficients as a function of latitude for NIWA-SOCOL of lower strato-spheric partial column ozone (black), transport-induced ozone trends (red) and chemistry-induced ozone trends (blue). The green line line is the non-linear contribution to ozone trends, and the grey line is the control line (sum of chemistry, transport and non-linear term). Light grey bars indicate the mid-latitude averaging region used in this study.
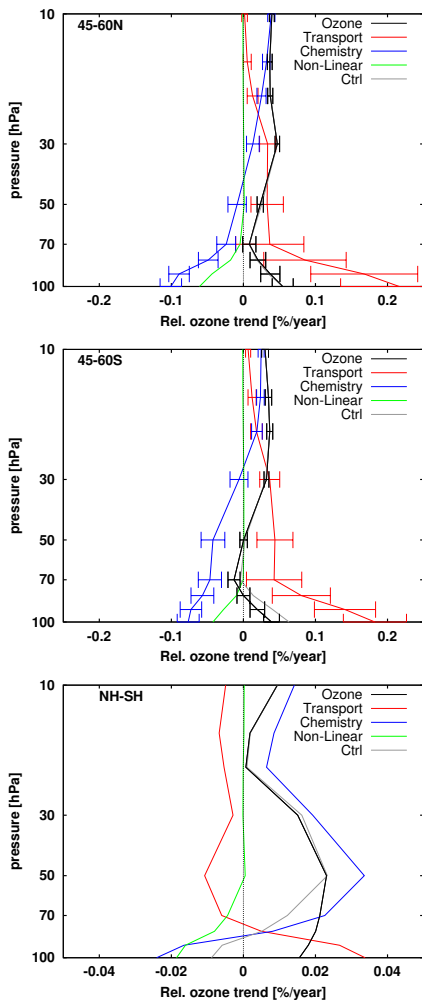
Fig. 9. As in Fig. 7 but for lower stratospheric ozone trends in NIWA-SOCOL.

Ozone return dates

H. Garny et al.
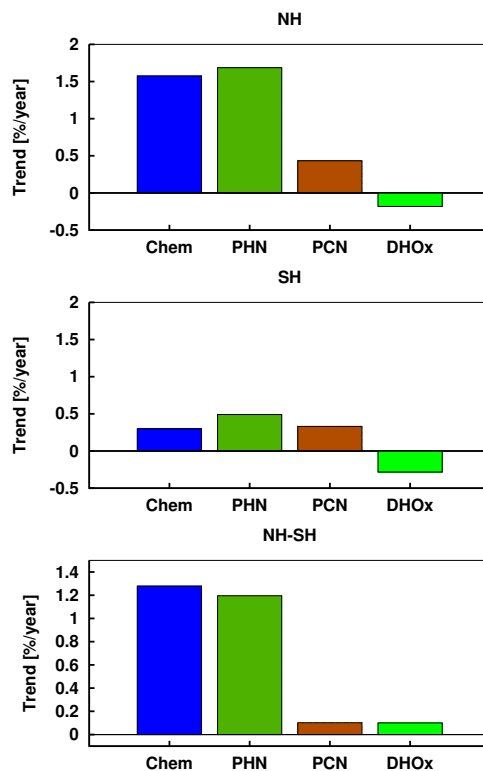
Fig. 10. Contributions to the chemically-induced ozone trends (blue bars) in the NH (top) and SH (middle) mid-latitudes, and the hemispheric difference (bottom), integrated between 250 and 300 hPa in E39CA. Reaction cycles are the production via $HO_2 + NO$ ("PHN") and $CH_3O_2 + NO$ (PCN), and the HO_x destruction cycle. The Chapman production cycles, NO_x and ClO_x destruction cycles are omitted since their contributions are close to zero.
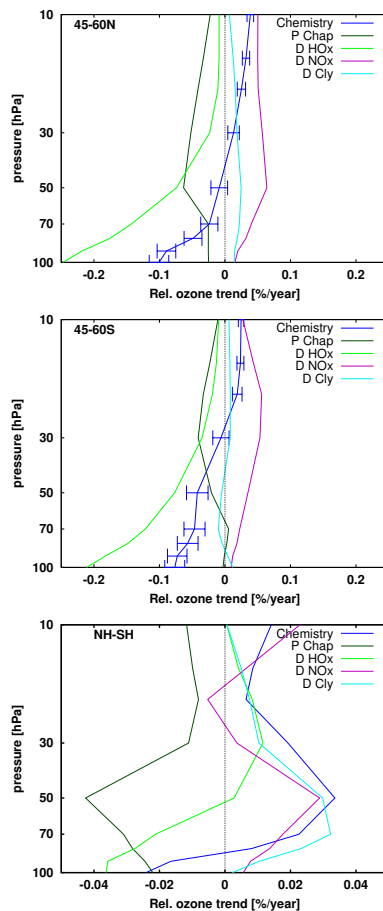
Fig. 11. As in Fig. 9 but showing the contributions of different reaction cycles (see legend) to the total chemically-induced ozone trend (blue).
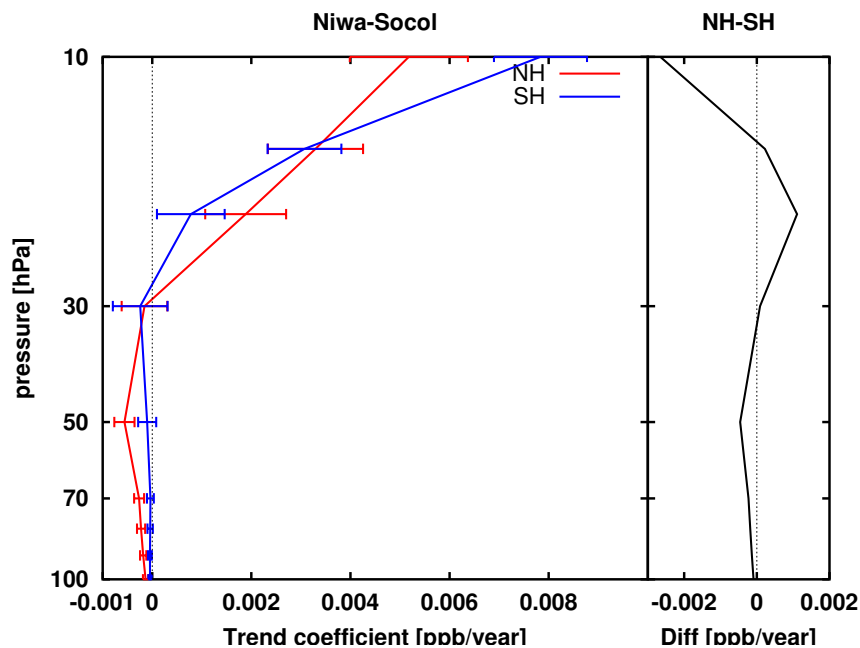
Fig. 12. Trend coefficients from NIWA-SOCOL of NO_x averaged over 45 to 60° N (red) and 45 to 60° S (blue) as a function of height. The error bars are the one σ uncertainties in the fit coefficients. The right panel shows the difference NH – SH.

Full Screen / Esc

Printer-friendly Version

Interactive Discussion
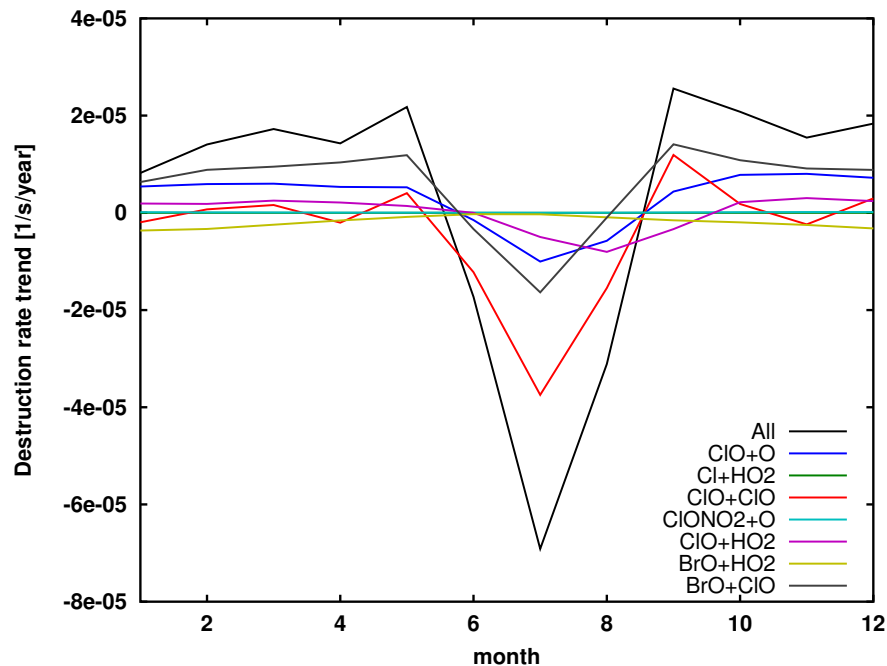
Fig. 13. Trend coefficients from NIWA-SOCOL of the destruction rates by the Cl_y cycles averaged over 45 to 60° S at 70 hPa of the sum of all reaction cycles (black line) and individual cycles (in color, as indicated by the legend).

Title Page

Abstract | Introduction

Conclusions | References

Tables | Figures

◄ | ►|

◄ | ►

Back | Close

Full Screen / Esc

Printer-friendly Version

Interactive Discussion

Temperature trend [K/year]

-0.04   -0.02   0   0.02   0.04
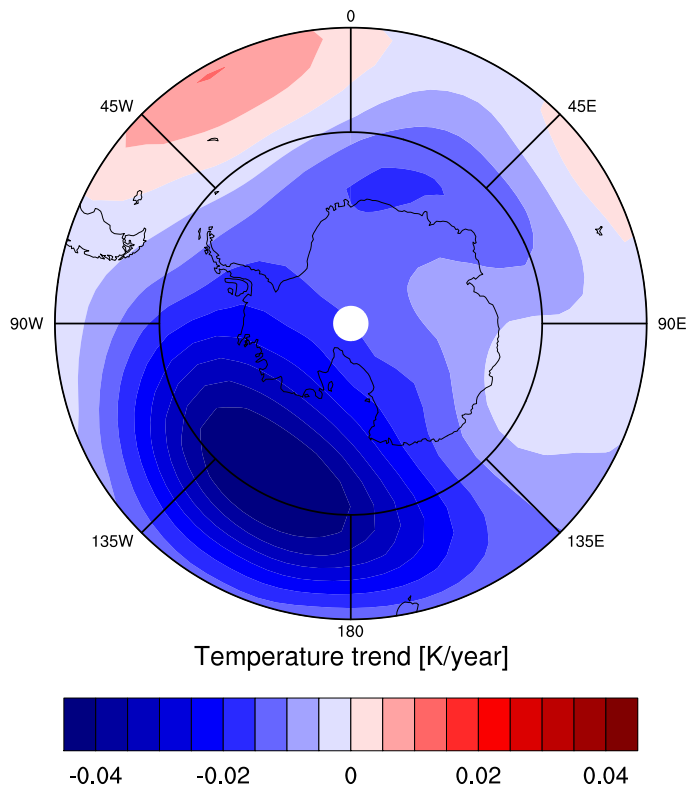
Fig. 14. Trends (1960 to 2049) in temperatures at 70 hPa in July from NIWA-SOCOL. The outer margin lies at 45° S, and 60° S is marked as black circle.

Title Page

Abstract   Introduction

Conclusions   References

Tables   Figures

◀   ▶

◀   ▶

Back   Close

Full Screen / Esc

Printer-friendly Version

Interactive Discussion
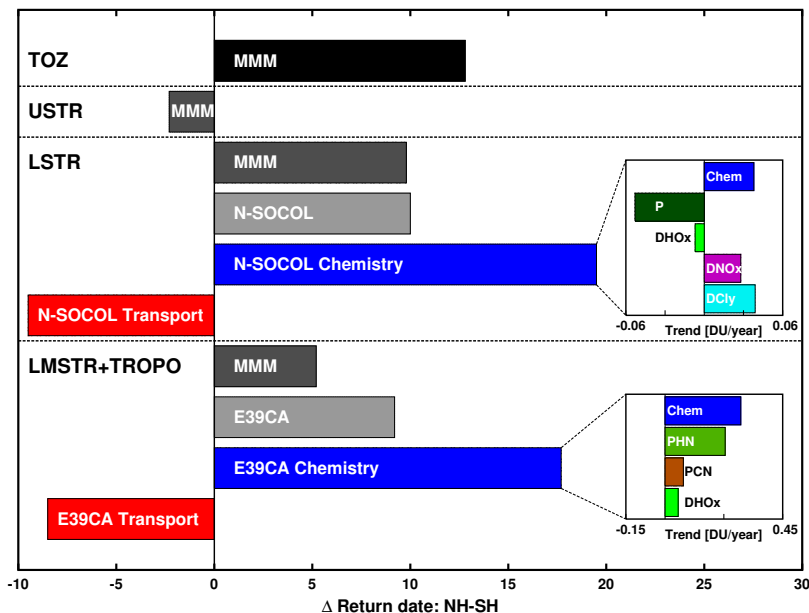
Fig. 15. Summary of the results: Hemispheric differences in mid-latitude return dates to 1980 values are about 13 yr in the multi-model mean (MMM) for TOZ. Upper stratospheric ozone contributed negatively to this difference, while return dates of lower stratospheric ozone (100 to 10 hPa) alone have a hemispheric difference of about 10 yr, and ozone below 100 hPa contributes another 5 yr. In the LSTR, in NIWA-SOCOL changes in chemistry only would lead to an earlier return in the NH of close to 20 yr, and changes in transport of ozone offset the chemical effects. Attribution of chemically-induced trends in the LSTR show that the earlier return of NH ozone is due to changes in the NO_x and Cl_y cycles. In the lowermost stratosphere and troposphere, hemispheric differences modeled in E39CA, somewhat above-average, are attributed to changes in chemistry, and transport offsets the chemically-induced changes. Enhanced production of ozone in the NH by the NO_x cycles is found to account for the stronger positive trend there.

Title Page

Abstract | Introduction

Conclusions | References

Tables | Figures

|◄ | ►|

◄ | ►

Back | Close

Full Screen / Esc

Printer-friendly Version

Interactive Discussion
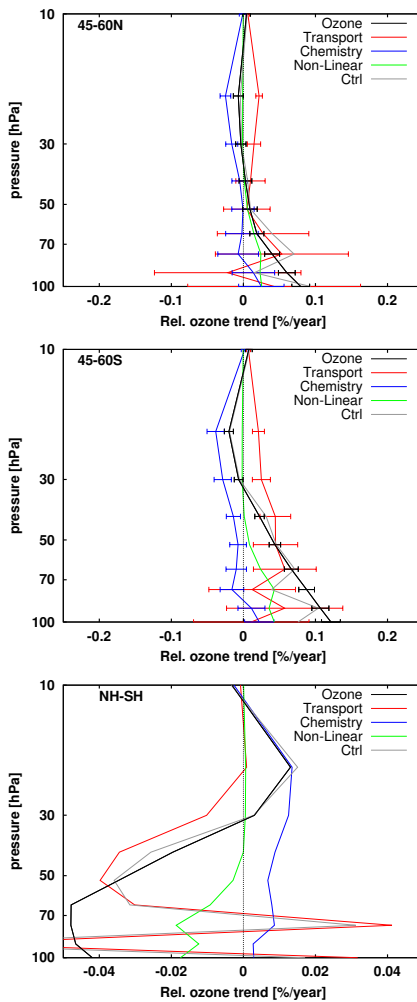
Fig. A1. As in Fig. 9 but for E39CA.

Ozone return dates

H. Garny et al.

◀ | ▶

◀ | ▶

Back | Close

Full Screen / Esc

Printer-friendly Version

Interactive Discussion
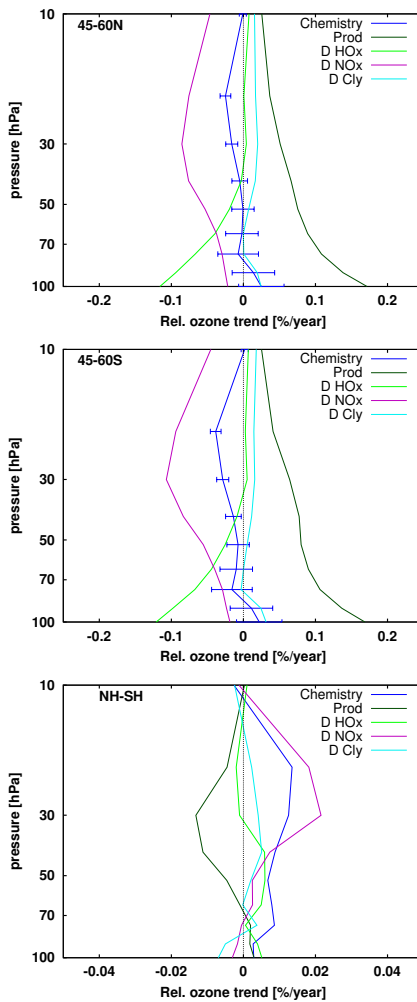
Fig. A2. As in Fig. 11 but for E39CA.

Ozone return dates

H. Garny et al.

Title Page

Abstract	Introduction
Conclusions	References
Tables	Figures

◄ | ►|

◄ | ►

Back | Close

Full Screen / Esc

Printer-friendly Version

Interactive Discussion
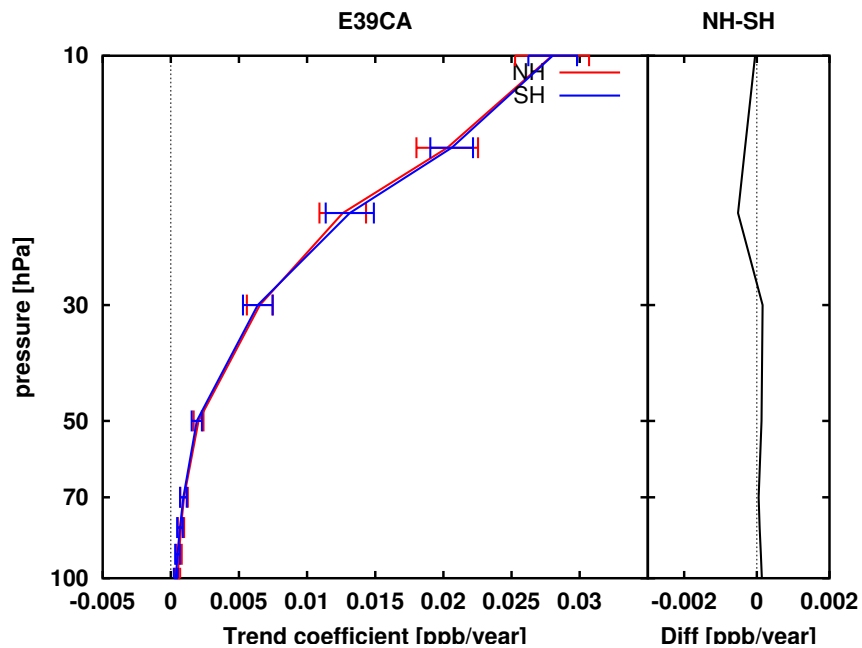
Full Screen / Esc

Fig. A3. As in Fig. 12 but for E39CA. Note the different x-axis scale.